ALMA MATER STUDIORUM – UNIVERSITÀ DI BOLOGNA
CAMPUS DI CESENA
DIPARTIMENTO DI
INGEGNERIA DELL'ENERGIA ELETTRICA E DELL'INFORMAZIONE
"GUGLIELMO MARCONI"

CORSO DI LAUREA MAGISTRALE IN INGEGNERIA BIOMEDICA

THE EFFECT OF INTERVERTEBRAL DISC SIMULATED DAMAGE ON THE HUMAN SPINE BIOMECHANICS.

(L'effetto della simulazione del danneggiamento del disco intervertebrale
sulla biomeccanica della colonna vertebrale umana)

Tesi in

MECCANICA DEI TESSUTI BIOLOGICI LM

Relatore

Chiar.mo Prof. Luca Cristofolini

Presentata da

Sara Montanari

Co-Relatore

M. Eng. Chloé Techens

Sessione III
Anno Accademico 2018/2019

A chi rallenta,

ma, nonostante le difficoltà, non si ferma

e arriva al traguardo.

Contents

Abstract

More than 50% of intervertebral discs in the third and fourth decade of life exhibit annular tears and fissures with different orientations and extents. On the other hand, *in vitro* biomechanical investigations of the disc surgery treatment, sometimes requires collaterals lesions, such as incision or disc material removal to recreate biological injuries, as in discoplastly. These lesions could have a mechanical impact on the spine flexibility and in the surrounding tissue and could alter the final outcomes of *in vitro* studies.

The influence of the presence of lesions on the biomechanics of the segment is still a debated research question.

Thus, this *in vitro* study aims to evaluate changes in spine biomechanics, in terms of stiffness, range of motion and disc height, induced by an increasing damage of human disc. In order to assess the impact of the annulus damage on the surrounding tissues, principal strain distributions were investigated in the lateral side opposite than the damaged region.

Eight fresh cadaver thoraco-lumbar FSUs were used in this study. The specimens were tested sequentially in flexion and extension in five different configurations: a) with the intact disc; b) with two vertical cuts; c) with four cuts, forming a square, without removing any part of the annulus; d) after having removed the cut part of the AF; e) after having removed the nucleus pulposus. Image analysis and surface strain distribution were performed on the lateral disc by means of the Digital Image Correlation.

Results showed that the IVD simulated damage of this study did not alter significantly the spine biomechanics: neither bending stiffness nor range of motion. The main effect caused by nucleotomy was the disc height reduction due to the lack of support caused by the nucleus loss. The strain distribution on the disc surface reflected the different vertebrae behavior related to their location in the spine. In both thoracic and lumbar segments, strains significantly changed in the last defect configuration, concentrating strains on smaller regions such as the mid-height line of the disc or along the endplates.

Riassunto

Più del 50% dei soggetti tra i trenta e quaranta anni presenta lesioni nell'anello fibroso dei dischi intervertebrali della spina dorsale. Anche studi *in vitro*, che mirano a valutare gli effetti di trattamenti chirurgici del disco intervertebrale sulla biomeccanica del rachide, possono richiedere lesioni, come incisioni o l'asportazione di parte del tessuto dell'anello fibroso, per ricreare le lesioni biologiche che sono oggetto di investigazione, come nel caso della *discoplastica*. Queste lesioni potrebbero avere un impatto meccanico sulla colonna vertebrale e sui tessuti circostanti e potrebbero quindi compromettere i risultati finali dello studio *in vitro*.

Le conseguenze della presenza di lesioni sul disco intervertebrale sul comportamento meccanico della spina dorsale rappresentano ancora oggi una questione di dibattito aperta. Questo studio *in vitro* ha quindi lo scopo di valutare gli effetti biomeccanici della colonna vertebrale, in termini di *stiffness*, *range of motion* e altezza del disco, come conseguenza di un crescente danneggiamento del disco. Inoltre per valutare come il danneggiamento dell'anello fibroso del disco si ripercuote sui tessuti circostanti, sono state analizzate le mappe di distribuzione delle deformazioni sul lato opposto alla regione danneggiata.

In questo studio sono stati utilizzati otto segmenti di rachide umano costituiti da vertebre toraciche e lombari. I provini sono stati testati sequenzialmente in flessione ed in estensione in cinque diverse configurazioni: a) con il disco intervertebrale intatto; b) con due tagli verticali nell'anello fibroso; c) con quattro tagli, formando così un quadrilatero, lasciando la parte tagliata *in situ*, d) dopo aver rimosso la parte di anello fibroso precedentemente tagliata; e) dopo aver rimosso il nucleo polposo. L'analisi delle distribuzioni delle deformazioni è stata eseguita nella regione del disco opposto alle lesioni, tramite l'utilizzo della *Digital Image Correlation.*

I risultati hanno mostrato come i danneggiamenti del disco, simulati in questo studio, non hanno alterato in maniera significativa né la *stiffness* né il *range of motion* dei segmenti analizzati. Il primo effetto osservato dopo la nucleotomia è stato la riduzione dell'altezza del nucleo, a causa della mancanza del supporto interno dovuto alla perdita del nucleo. La distribuzione delle deformazioni sulla superficie del nucleo rispecchia il diverso

comportamento delle vertebre in relazione alla loro posizione nel rachide. Sia nel caso di segmenti toracici che lombari è stato possibile osservare un significativo cambiamento della distribuzione delle deformazioni dopo l'esecuzione dell'ultimo difetto, che ha portato alla concentrazione delle deformazioni in piccole regioni come il centro del disco o lungo gli *endplates.*

Chapter 1

Introduction

The intervertebral disc impacts significantly in load distribution on the adjacent vertebral bodies and in the entire spine motion [Newell *et al., 2017*].

An analysis of midsagittal sections of cadaveric specimens, conducted by Krismer *et al, 1997*, showed that more than 50% of intervertebral discs in the third and fourth decade of life exhibit annular tears and fissures with different orientation and extents.

Also, *in vitro* biomechanical investigation of the disc surgery treatment, requires sometimes collateral lesions, such as incision or disc material removal, to recreate a particular biological condition, as in Percutaneous Cement Discoplasty. These lesions could have a mechanical impact on the spine stability and on the surrounding tissue and could alter the final outcomes of the *in vitro* study.

The consequences and influence of the presence of lesions on the biomechanics of the motion segment are still a debated research question.

It is generally admitted that the disc disruptions and tears are the main factors responsible for the clinical instability [Kirkaldy-Willi *et* Farfan, *1982*] but this statement is not supported by available biomechanical studies [Galbusera *et al., 2014*]. For example, Tanaka *et al., 2001,* showed an increased flexibility of human spine segments exhibiting biological radial tears, but the simultaneous presence of other degenerative changes in the investigates specimens did not allow to distinguish the specific mechanical effect of tears. Thompson *et al., 2000,* observed a correlation between rim lesions and reduced stiffness in flexion and extension which may be linked to a loss of nucleus pulposus pressure.
Thompson *et al, 2004,* determined the mechanical effect of individual concentric tears, radial tears and rim lesions of the ovine annulus, but in their study subsequent tears were introduced in locations that minimized communication between lesions.

Therefore, as Galbusera *et al.*, concluded in their work in 2014, although the literature suggested that the degenerative changes of the intervertebral disc and surrounding structures lead to subtle alterations of the mechanical properties of the functional spinal unit (FSU), supporting a general increase of spinal instability with disc degeneration could not be found.

1.1 Anatomy of the human spine

The spine is the supporting structure of human body and it has three main biomechanical functions:

- It supports loads and transfers weights and resulting bending moments of head, trunks and pelvis providing structural support and balance to maintain an upright posture;
- It allows the physiologic movements of head, trunk and pelvis, and, in particular, it allows the relative rotation between the vertebral bodies while preventing their translation;
- It protects spinal cord, nerve roots and several of the body's internal organs and it reduces the transmission of accelerations from the lower limbs to the internal organs.

The spine consists of 33 vertebrae which according to their position are subdivided into *cervical* (7 vertebrae, C1 . C7), *thoracic* (12 vertebrae, T1 – T12), *lumbar* (5 vertebrae, L1 – L5), *sacrum* (5 fused vertebrae) and *coccyx* (4 fused vertebrae) (*Figure 1.1*).

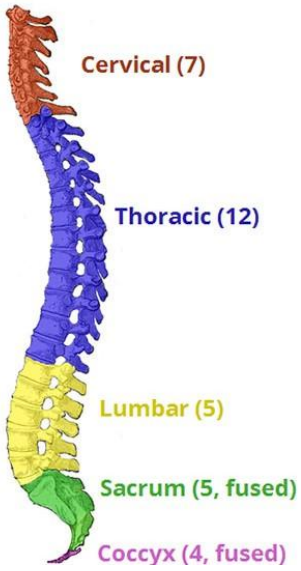

Figure 1.1-
Spine sagittal view.

A vertebra consists in two essential parts:

- the *body*, the anterior segment;
- the *vertebral* or *neural arch*, the posterior part, which consists in two *pedicles* and two *laminae*, and supports seven *processes*: four *articular*, two *transverse* and one *spinous*;

These two parts enclose a foramen, called the *vertebral foramen*. The vertebral foramina constitute canals for the protection of the *spinal cord*. The *intervertebral foramina* are two apertures between every pair of vertebrae, one on either side, for the transmission of the spinal nerves and vessels [Gray, *2016*], (*Figure 1.2*).
Vertebrae are connected by intervertebral disc and ligaments.

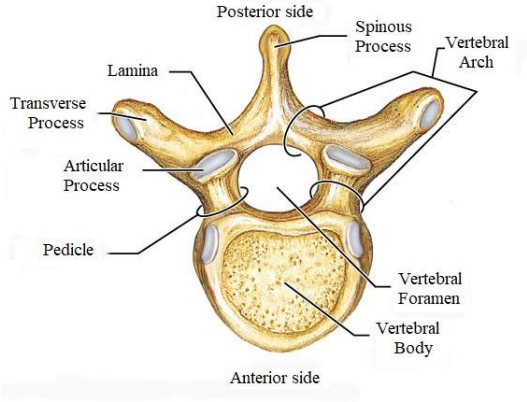

Figure 1.2 - *Axial view of a vertebra.*

1.1.1 Intervertebral discs

Intervertebral discs (IVDs) are the main joints of the spinal column and represent one-third of its height. Their major role is mechanical, as they constantly transmit loads arising from body weight and muscle activity through the spinal column. They provide flexibility to the spine , allowing spine motion. The intervertebral discs are complex structures that consist in a thick outer ring of fibers called the annulus fibrosus (AF), which surrounds a more gelatinous core known as the nucleus pulposus (NP); the nucleus pulposus is interposed inferiorly and superiorly by cartilage endplates (*Figure 1.3*).

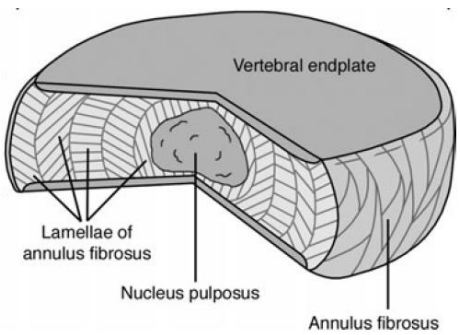

Figure 1.3 - *A cut out portion of an intervertebral disc [Prithvi Raj, 2008].*

The annulus fibrosus is composed of a series of 15 to 25 concentric lamellae of fibrocartilage, with the collagen fibers lying parallel within each lamella. The lamellae are approximately 0.05-0.5 mm thick, and the thickness increases from outer to inner layer. Approximately 48% of the lamellar layers are circumferentially incomplete and the percentage of incomplete layers increase with age. [Newell *et al., 2017*]. The fibers are oriented approximately 60° to the vertical axis , alternating between the left and right orientation in adjacent lamellae. Elastin fibers lie between the lamellae, helping the disc to return to its original arrangement following bending [Prithvi Raj, *2008*].

The nucleus pulposus forms the core of the intervertebral disc and it is located slightly posteriorly as the lamellae of the annulus fibrosus are thinner and less numerous in the posterior side [Adams *et al., 2014*]. The NP is a gelatinous structure that accounts for 40-50% of the volume of the adult disc and 25%-50% of the transverse cross-sectional area. The NP has such a high water content that it exhibits a hydrostatic pressure which increases in response to compressive loading, and this pressure generates tension in the surrounding AF. Its main constituents are proteoglycan, collagen and water [Newell *et al., 2017*].
The boundary between NP and AF is very distinct in the young individuals; but during growth and skeletal maturation, it becomes less obvious, and increasing age the nucleus generally becomes more fibrotic and less gel-like [Prithvi Raj, *2008*].

Finally, the cartilage endplates are a thin horizontal layer of hyaline cartilage. These interface the disc and the vertebral bodies. The collagen fibers run horizontal and parallel to the vertebral bodies, with the fibers continuing into the disc [Prithvi Raj, *2008*].

The mechanical functions of the disc are given by the extracellular matrix of the annulus; its composition and organization govern the disc's mechanical responses. The main mechanical role is provided by the two major macro-molecular components (*Figure 1.4*):

- Collagen, present mostly as type I and type II fibrils; it provides tensile strength to the disc and anchors the tissue to the bone;
- Proteoglycan, which is the responsible for maintaining tissue hydration and gives the osmotic pressure to the nucleus. The proteoglycan and water content of the nucleus is larger than in the annulus.

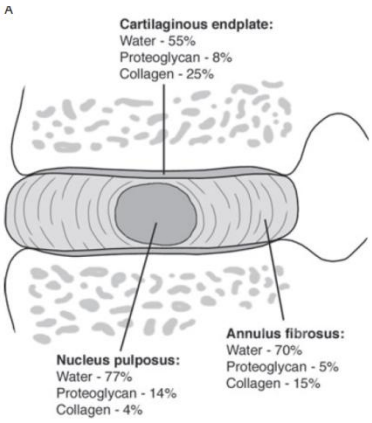

Figure 1.4 - *Biochemical composition of the nucleus [Prithvi Raj, 2008].*

1.2 Intervertebral disc tears

1.2.1 Types of lesions

Annular lesions are feature of IVD degeneration and that may precede morphological changes in the nucleus (Osti *et al., 1990*) and instigate changes in cellular activity that are consistent with IVD degeneration.

Annular lesions are defined as disruption of the arrangement of the annular fibers and can be distinguished in (*Figure 1.5*):

- *Concentric tears*: circumferential lesions found in the outer layers of the annulus which represent splitting between adjacent lamellae of the annulus [Adams *et al., 2014*]; they are most prominent in the anterior periphery of the disc [Thompson *et al., 2004*];
- *Radial tears:* irregular radial fissures that begin within the center of the disc (NP) and progress in radial direction either in the transverse plane or in a cranio-caudal direction [Adams *et al., 2014*]. They tend to appear in the posterior or postero-lateral part of disc [Thompson *et al., 2004*];
- *Rim lesions*: are defined as a separation of the outer annulus from the vertebral rim of the adjacent vertebral body. They more commonly happen in the anterior annulus [Thompson *et al., 2004*].

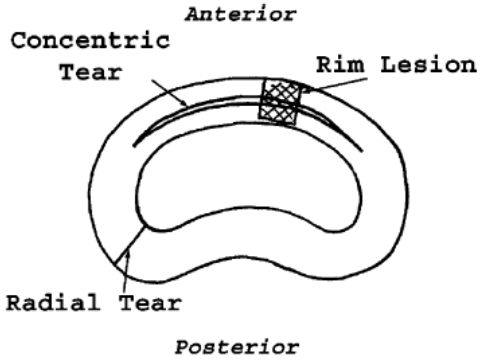

Figure 1.5 - *Annular tears [Thompson et al., 2004].*

1.2.2 Intervertebral disc tears: state of the art

A literary review was performed in order to understand how, in the last years , research tried to understand the damaged disc behavior simulating lesions on it.

Only *in vitro* human works were taken into account, excluding animal studies and finite element models, as shown in details in Appendix A

The majority of the studies removed partially or totally the nucleus pulposus from the disc postero-lateral region, only Goel *et al., 1986*, incised the posterior side of the disc, and Tencer *et al., 1982*, created staggered horizontal cuts around the disc circumference, near both endplates.

Lee *et al., 2018*, and Shea *et al, 1994*, made a circular hole in the annulus; whereas a square or a rectangular window was realized by Bostelmann *et al., 2015*, Kuroki *et al, 2004*, Seroussi *et al., 1989*, and by Panjabi *et al., 1984.*
All the other authors impacted the annulus fibrosus with different types of lesions: with a cruciform incision (Cleason *et al., 2019,* Showalter *et al., 2014*, O'Connell *et al., 2011*), an oblique incision oriented along the fiber direction (Heuer *et al. in 2007 and 2008*, and Krismer *et al. in 1996*), an horizontal incision (Ivicsics *et al., 2014*, and Goel *et al., 1986*) or with a vertical cut in Frei *et al, 2001,*. study.

In almost all the studies, the spine segment was loaded with an axial compression, or under pure bending in flexion and extension in some cases.

Many studies recorded the intradiscal pressure to register pressure variations inside the disc due to annulus fenestration and nucleus removal.

Range of motion was computed in six studies (Lee *et al., 2018*, Bostelmann *et al., 2015*, Heuer *et al., 2008*, Heuer *et al., 2007*, Kuroki *et al., 2004*, and Goel *et al., 1986*). In all cases pins, markers and dial gauges were attached on the vertebral bodies, and their displacements were tracked by 3D motion analysis system or laser scanner. Heuer *et al, 2007*, used a rotational potentiometers.

Internal disc deformation field and disc surface strains were both mainly acquired by imaging system as MRI (Cleason *et al, 2019*, Showalter *et al., 2014*, O'Connell *et al., 2011*) and laser scanner (Heuer *et al., 2008*). Only Frei *et al, 2001*, used triaxial strain gauges.

Load and displacement data were mainly acquired by displacement sensors, LVDT and potentiometers transducers.

1.3 Strains measurement over the disc surface

Strains analysis over the intervertebral disc surface has been a challenge through the years.

Although strain gauges are not recommended on the intervertebral disc because the discs have a low elastic modulus, few studies in literature used this method [Frei *et al, 2001;* Gustafson *et al, 2016*].

In general, due to the disc composition, studies that have been carried out to measure strains have used image-based methods. Heuer *et al., 2008*, used a laser scanner to acquire surface roughness, O'Connell *et al*., Showalte*r et al*., and Cleason *et al*., used a MRI system. Similarly, Karakolis *et* Callaghan, *2015*, extracted strains distribution by means of high resolution images.

Spera *et al*, in 2011, proposed a Stereo-Digital image correlation: a full-field measurement system recordings over more than 180° of the IVD surface was achieved by sequentially moving a single camera through fixed positions in order to cover the desired angle of vision. Their method does not seem applicable to segment comprising both hard and soft tissue [Ruspi *et al., 2017*].

Recently, the feasibility of measuring the full-field strain distribution in the vertebrae and disc by means of Digital Image Correlation was successfully demonstrated [Palanca *et al., 2018*].

1.3.1 Digital Image Correlation

The Digital Image Correlation (DIC) is a contact-less, non invasive optical method for measuring surface displacement and strain of materials subjected to mechanical stress [Palanca *et* Brugo, *2015*]. The method compares two images of the same specimen before and after deformation, acquired by mean of one (to obtain a two-dimensional outcome) or two cameras. Through two cameras, a three-dimensional outcome is obtained exploiting the concept of stereoscopic view of human vision: the final image is gained by merging two projection of the same scene obtained from two different points of view. The specimen must be illuminated by white homogeneous lights during the test (*Figure 1.6*). An accurate calibration of the image system prior to the measurements is a crucial point for ensuring the reliability of the measured data [Siebert *et al., 2007*].

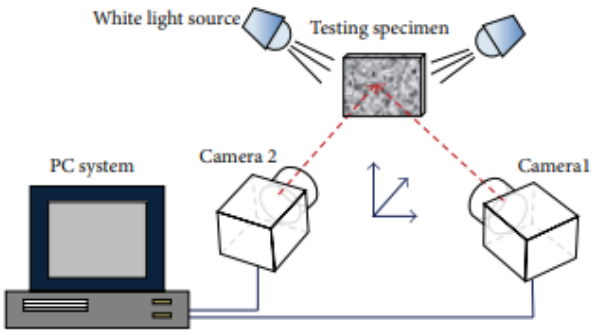

Figure 1.6 - *A schematic plot of a DIC testing setup [Liao et al., 2014].*

The correlation of digital images is based on the acquisition of a set of frames of the specimen at various stages of deformation (from the unload condition, the reference, to the stressed condition). The specimen surface is covered with a randomized speckle pattern, which is applied as a stochastic texture to the object before the measurements. After the acquisition, each object point on the specimen surface is identified based on the pattern [Siebert *et al.,* 2007]. A correlation algorithm identifies corresponding points in the two cameras images by subdividing the first camera image into small sub-images, called *facet*. The correlation algorithm determines a suitable transformation of each of the

facets, which matches the homologous area in the second camera image. These transformations are determined for every loading step of the specimen under test. The displacement field is then computed, and subsequently, the strain filed is obtained by derivation. The size and the spacing (*grid spacing*) of these facets can be varied, influencing accuracy and speed of evaluation [Palanca *et al., 2016*] (*Figure 1.7*).

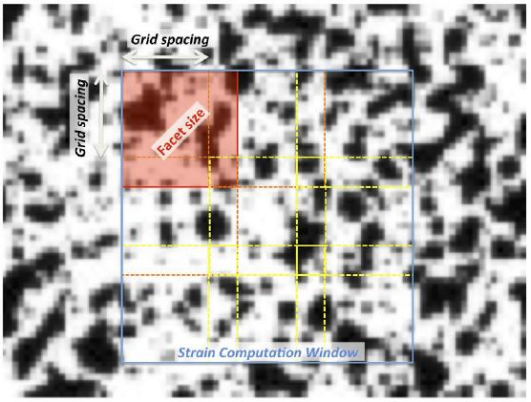

Figure 1.7 *– Detail of the specimen surface prepare with a random speckle pattern with facet parameters highlighted [Palanca et al., 2016].*

1.4 A recent surgical treatment: Percutaneous Cement Discoplasty

Percutaneous Cement Discoplasty (PCD) is a novel minimally invasive technique fror the treatment of 'vertical instability' (dynamic foraminal stenosis) in patient who are not suitable for a more invasive surgical procedure, such as the gold standard treatment of degenerative disc disease.

Varga *et al*., presented this technique in 2015, as a surgical treatment to recover the disc height and free the nerve after its compression due to the vacuum phenomenon inside the intervertebral disc resulting in the collapse of the adjacent vertebra. PCD consists in filling the empty disc with an injection of acrylate cement. Varga *et al., 2015*, reported their clinical study on 47 patients showing a significant improvement of their quality of life. Sola *et al., 2018*, presented a surgery of a patient treated with PCD, and the following year, Kiss *et al., 2019*, showed the recovery of the lumbar alignment in 27 patients after a discoplasty surgery.

Thus, only few studies in literature report PCD surgery cases, and the impact of this new technique on the human spine biomechanics has not yet been investigated.

An ongoing study [Techens *et al.*, 2020] assessing mechanical consequences of PCD on lumbar spine stability, simulated the vacuum degenerated disc with an annular fenestration and a manual nucleus pulposus removal.
The influence of this disc damage on the AF behavior and the spine biomechanics is unknown.

1.5 Aim of the study

Because of the consequences of lesions presence of on the biomechanics of the motion segment are still not clear, this work aimed at enlarging the knowledge about this research question.

The aim of this *in vitro* study was to evaluate changes in spine flexibility, in terms of stiffness, range of motion and disc height, as a consequence of sequentially increasing the IVD damage, in order to:

i. Elucidate if there is a specific degree of damage where the biomechanics of the IVD is substantially altered;
ii. Explore the artifacts induced by simulated disc lesions, e.g. when studying discoplasty.

In addition, the impact of the annulus damage on the surrounding tissues was assessed using Digital Image Correlation to study the surface strains.

Chapter 2

Materials and Methods

This *in vitro* study has been conducted at the laboratory of Biomechanics of the Department of Industrial Engineering (University of Bologna).

For this study eight thoraco-lumbar spine segment were prepared simulating five disc defect configurations, starting from the intact disc and increasing the damage until the complete removal of the NP. All the specimens were tested sequentially in flexion and extension in all configurations with repeated measurements. DIC was used to acquire true principal strain distributions on the disc surface. Disc height was measured on the DIC images. In addition, Range of Motion and stiffness were computed to analyze the flexibility of the spine. Statistical analysis was performed to assess the result significance.

2.1 Specimens preparation

Fresh cadaver thoraco-lumbar functional spine units (FSUs) were used in this study, under ethical committee approval. A FSU consists of two adjacent vertebrae with the intervertebral disc and ligaments intact between them; it is a common specimen length used for modeling the mechanical behavior in a given region of the spine [Wilke *et al., 1998]*].

The spines, coming from six donors aged from 53 to 77years old, were separated into eight FSU testing specimens. (*Table 2.1*).

Sp. N°	Testing Donor	Level	Gender	Age at death (years)	Height (cm)	Body Weight BW (Kg)	Cause of Death
#1	62	T9 - T10	F	77	155	43	Cancer
#2	62	T11 - T12	F	77	155	43	Cancer
#3	63	T10 - T11	M	68	173	82	Cardiac failure
#4	66	L4 - L5	M	79	193	79	Alzheimers dementia
#5	67	T12 - L1	M	53	183	82	Brain cancer
#6	68	T10 - T11	M	59	188	101	Pneumonia
#7	68	T12 - L1	M	59	188	101	Pneumonia
#8	71	T10 - T11	F	58	158	132	Shoulder and skin cancer

Table 2.1 - Specimen information.

2.1.1 CT scans of the specimens

Before starting the specimens cleaning, CT scans were performed for all the spines, except the #6 and #7. CT scans were performed in a private hospital at Villalba (BO), and images were acquired by the scanner Aquilion, ONE, Toshiba, with a current of 200mA, a voltage of 120 kV and a 0.5 mm voxel. CT scans were observed to:

- Assess the initial condition of the specimens;
- Chose the exact levels for the study;
- Compute the offset for the load application;

From the CT images a fusion at the IVD level was seen between the T11 and T12 vertebrae in the specimen #2 and a fracture of the posterior process was discovered in the L5 and T10 vertebrae, on the #4 and #8 spine, respectively.

2.1.2 Cleaning of the specimens

The FSUs were prepared in accordance with accepted procedures defined by Wilke *et al.,1998*. All the specimens were stored sealed in a double plastic bags at -28°C; these storage conditions do not have any effect on viscoelastic biomechanical properties [Panjabi *et al., 1985*].

After having thawed the specimens in water at room temperature, the whole specimens were grossly cleaned detaching the most of soft tissues (skin, fat and muscles) covering the bone by surgical spoons and pincers (*Figure 2.1*). At this point, it was easier to identify the levels of interest, so the FSUs were separated cutting through the intervertebral disc adjacent to the vertebral bodies using the scalpel and the saw (*Figure 2.1*). FSUs cleaning war completed detaching the smallest part of soft tissues by scalpel and forceps, taking care to leave intact the anterior longitudinal ligament, the posterior longitudinal ligament, and the facet joints.

Figure 2.1 – *Surgical instruments used for the specimens cleaning: a) surgical spoon, b) scalpel, c)needle holder, d)pincer, e)saw.*

Because of the broken posterior processes (PP) of two FSUs, the PP were cut in all the specimens, to have the same condition for all of them. Posterior processes were cut at the facet joints level (*Figure 2.2*), in this way a small part of the PP and of the interspinous ligament kept, while the supraspinous ligament was totally removed. In addition bone fusion and ostheophytes were removed in the specimen #1 and #2 without damaging the disc.

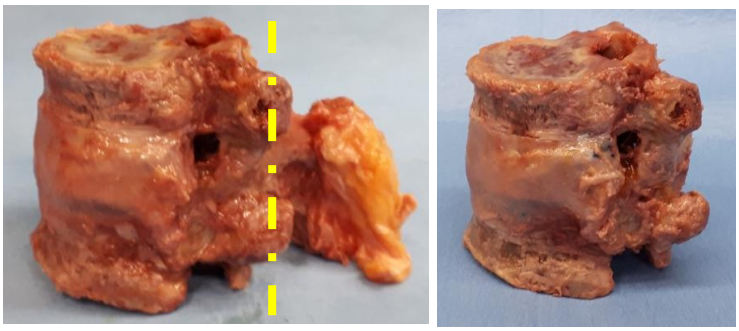

***Figure 2.2**- FSU after the cleaning procedure. Left: FSU with the posterior process and the supraspinous ligament intact; the yellow line is the cut level to remove the PP. Right: FSU after the PP cut.*

2.1.3 Alignment of the specimens

To ensure that the specimen can be mounted in the testing machine in a repeatable way [WIlke *et al., 1998*] and that mechanical loading is applied appropriately to all the FSUs [Newell *et al., 2017*], it is important for motion segments to be secured in a fixative pot. In order to facilitate the anchoring of the specimen to the pot, all the soft tissues were removed from the vertebral endplates and cortical surfaced to within at least 1 cm of the endplates margins (*Figure 2.3*). In addition, screws were partially inserted into the cortical bone at cranial and caudal extremities (*Figure 2.3*), so that the screws heads were embedded in the cement. One, two or three screws were inserted in each extremity according to the size of the vertebral body and the surface of the endplate.

***Figure 2.3** - Specimen with screws in the vertebral body extremity; soft tissues were totally removed from the vertebral endplate and cortical surface.*

Indeed, in order to test the specimen under the same conditions of load the FSUs were aligned with the intervertebral disc horizontal following a reproducible and suitable procedure already existing.

To obtain a stable alignment with the horizontal disc either in the frontal view either in the lateral view a 6 Degree of Freedom (DoF) test system (*Figure 2.4*) was used. One extremity of the FSU was clamped with the anterior side in front of the operator on the 6 DoF test system. With the help of a caliper the middle line of the disc was marked; that was aligned horizontally in the transverse plane. Then it was aligned horizontally also in the sagittal plane.; using the set square and the horizontal rules.

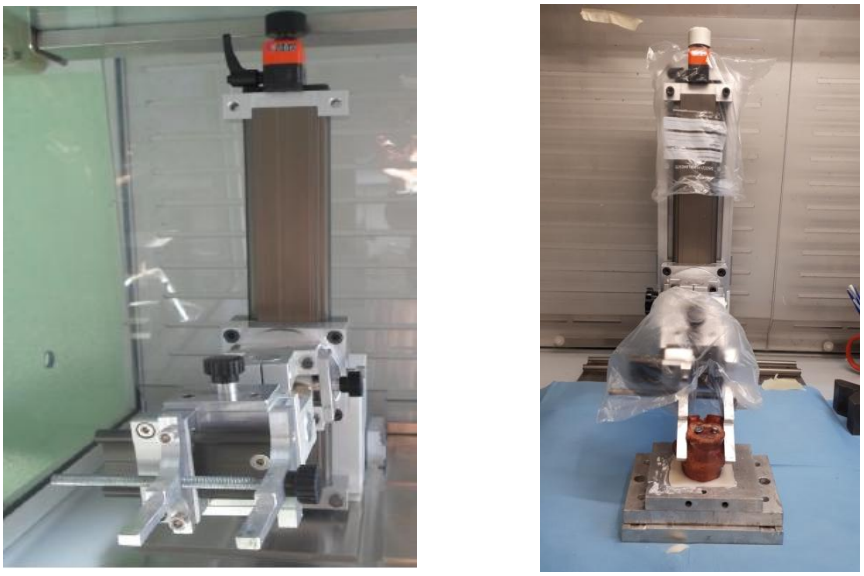

Figure 2.4 *- Left: 6 DoF system;*
Right: specimen clamped in the 6 DoF and embedded into cement inside a metallic pot.

Then the specimen was embedded into cement for 20 minutes, inside a metallic pot with a square hole (*Figure 2.4*). After the cement hardened, the specimen was turned clamping the cemented extremity on the 6 DoF. The previous procedure was repeated aligning upper and lower pots using the square set to be sure to have both pots horizontal and parallel.

Both extremities of the FSUs were potted with radiopaque Tecres cement, by mixing cement powder (PMMA) and the related monomer (MMA) in a ratio of 2:1.

In this way two cemented basis parallel to each other at both extremities of each FSU were created, with the horizontal intervertebral disc (*Figure 2.5*).

Figure 2.5 - *FSU with the cemented basis at both extremities.*

2.1.4 DIC Speckle - Pattern

In order to measure surface strains of specimens with Digital Image Correlation (DIC) system a white-on-black speckle pattern was sprayed on the lateral side of the specimens. The side was chosen randomly, but attention has been paid to having, finally, half specimens with the left side painted and the other half with the pattern on the right side (*Table 2.2*). This was important to avoid that results depend on the side where defects were executed or on the side where the deformations were acquired.

Sp. N°	Background side
#1	Left
#2	Left
#3	Left
#4	Right
#5	Right
#6	Right
#7	Right
#8	Left

Table 2.2 – *Painted side of each specimen.*

The dark background was prepared painting the lateral side of the FSUs with a saturated solution of methylene blue, obtained mixing 25 ml of water and 1 g of methylene blue powder (Farmalabor).

Three layers of paint were deposited on the specimen with a soft brush to be sure the background was dark enough without impacting the properties of the disc [Palanca *et al., 2018*] (*Figure 2.6*).

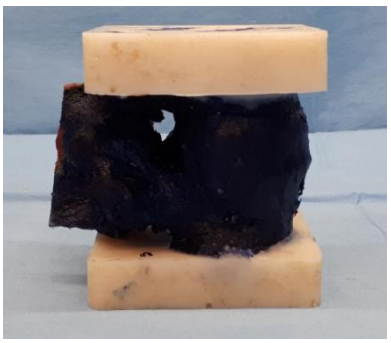

Figure 2.6 - *Specimen with the blue background.*

In order to apply the speckle-pattern on the specimen's surface an airbrush gun (AZ3 THE 2, nozzle 1.8 mm, Antes Iwata, Italy) (*Figure 2.7*) was used with a solution of water-based paint (Q250201 Bianco Opaco, Chrèon, Italy) and water.

Figure 2.7 *- Airbrush gun; the red circle markes the airflow knob.*

Dot size have been previously optimized [Ruspi *et al., 2018*] in order to reach the 50:50 proportion of black-white color (every single dots should have a dimension of 3-5 pixels). According to specimen sizes and lenses used:

- 20 ml of white paint were mixed with 8 ml of water;
- The air pressure was set at 1 bar;
- The airflow knob of the airbrush gun was opened with 4 turns (*Figure 2.7)*;
- The white paint was sprayed holding the airbrush around 30 cm from the specimen.

The optimized pattern resulting is shown in the figure below (*Figure 2.8*).

Figure 2.8 *- Speckle pattern on the lateral side of the specimen.*

2.1.5 Defects of the disc

In order to explore how disc defects and lesions impact the spine biomechanics, the IVD tears (*Figure 2.9*) were gradually increased, starting from the intact disc as control condition.

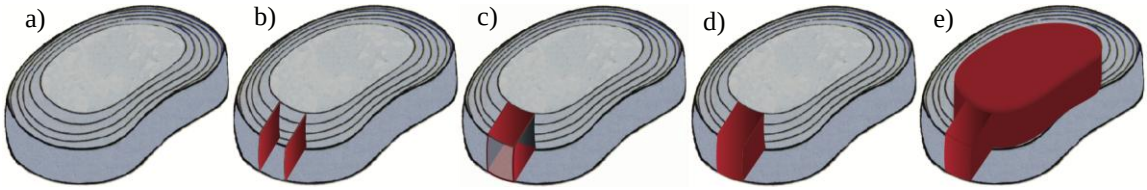

Figure 2.9 –
IVD tears in the different configurations; the red parts represent the cuts and the removed materials.

All the specimens were sequentially tested in these five configurations:

a) *With the intact disc*;
b) *With two vertical cuts on the annulus fibrosus (Figure 2.10)*: Two vertical cuts were made in the lateral side of the disc with a number 11 scalpel blade, from the upper endplate to the lower endplate. The annulus has been cut to reach the nucleus. The *table* shows the size of the cuts;

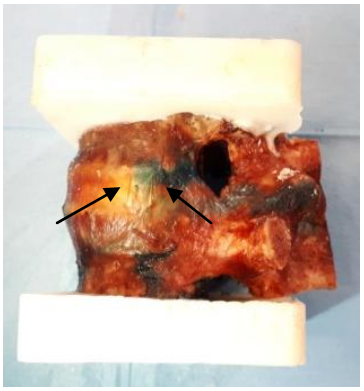

Figure 2.10 - *Specimen with the two vertical cuts.*

c) *With four cuts, forming a square, without removing any part of the annulus (Figure 2.11)*: Two additional horizontal cuts were made to separate the annulus from the endplates between the two previous vertical cuts, with a number 11 scalpel blade;

Figure 2.11 - *Specimen with two additional horizontal cuts.*

d) *With a square hole in the annulus (Figure 2.12)*: The annulus square plug between the four previous cuttings was removed with a rongeur: in this way the nucleus was visible through the hole;

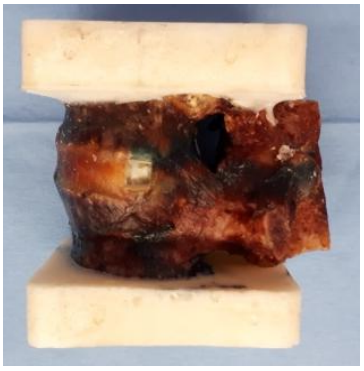

Figure 2.12 - *Specimen with the square hole in the annulus; the nucleus is visible through the hole (white part).*

e) *Without the nucleus pulposus (Figure2.13)*: through the annulus window created in the previous configuration, as much nucleus as possible was removed with a curette and a surgical spoon. Each specimen was weighed before and after the nucleotomy to assess the amount of nucleus removed (*Table 2.3*).

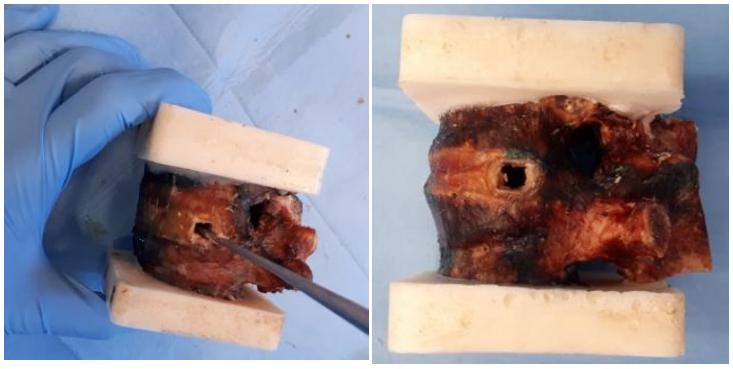

Figure 2.13 - *Left: Removing of the nucleus by means a curette; Right: specimen without the nucleus pulposus.*

Sp. N°	Lenght of cuts (cm)	Distance between cuts (cm)	Nucleus removed (g)
#1	0,51	0,42	1,80
#2	0,52	0,62	2,80
#3	0,66	0,53	3,40
#4	1,66	1,05	8,90
#5	0,87	0,54	5,40
#6	0,50	0,56	2,90
#7	0,85	0,59	3,50
#8	0,65	0,59	1,70

Table 2.3 *- Sizes of cuts executed in the configuration b) and amount of nucleus removed in the configuration e).*

All the defects were executed manually in the opposite side to that observed by the DIC and in order to reduce the variability between different test sessions. The disc lesions were produced directly on the testing machine up to configuration d). Removing all the nucleus pulposus from the FSU on the testing machine was not possible, so that the nucleotomy and the associated tests were performed at a later time.

2.1.6 CT measurements

In order to apply the load in a pre-defined and reproducible position, according to the protocol described in the following section, anatomical measurements were made on the disc under study, in particular the antero-posterior length and the lateral width of the IVD. Measurements were taken on CT images, using the free software RadiAnt DICOM Viewer 5.5.0. The midplane of the disc was located in the sagittal plane by defining the disc height where it appeared the highest. In the transverse plane, at the disc midplane, the anterior-posterior length (*L*) was measured in the center of the disc, and the disc width (*W*) was measured as the lateral length in the center of the disc (*Figure 2.14*). Each quantity was measured three times and means were considered (*Table 2.4*).

Sp. N°	Level	*L* (cm)	*W* (cm)
#1	T9 - T10	2,43	3,02
#2	T11 - T12	2,66	3,55
#3	T10 - T11	2,99	4,10
#4	L4 - L5	4,94	6,64
#5	T12 - L1	3,35	4,87
#6	T10 - T11	***3,74***	***4,39***
#7	T12 - L1	***3,85***	***4,51***
#8	T10 - T11	2,34	3,41

Table 2.4 *–Disc length and width values based on CT images; the bold numbers represent the computed values for the specimens without CT scan.*

Could not be applied to the specimens number #6 and #7, as CT scans were not available for these. For these FSUs the disc width (*W*) was measured on the specimens with a caliper. To obtain the disc length (*L*), the distance (*D*), between the anterior part of the disc and the posterior one, was manually measured with a caliper; this distance was greater than the real disc length. In order to evaluate the discrepancy between *L* and *D*, both these measures were taken on the CT images (*Figure 2.14*) of the same levels of the #6 and #7 FSUs. An error of 5% was found for the T10-T11 level and an error of 10% resulted for the T12-L1 level. So, to obtain a reliable value for the #6 and #7 FSUs disc height *L*, the 5% and the 10% respectively, was subtracted from the measured values (*D*) (*Table 2.4*).

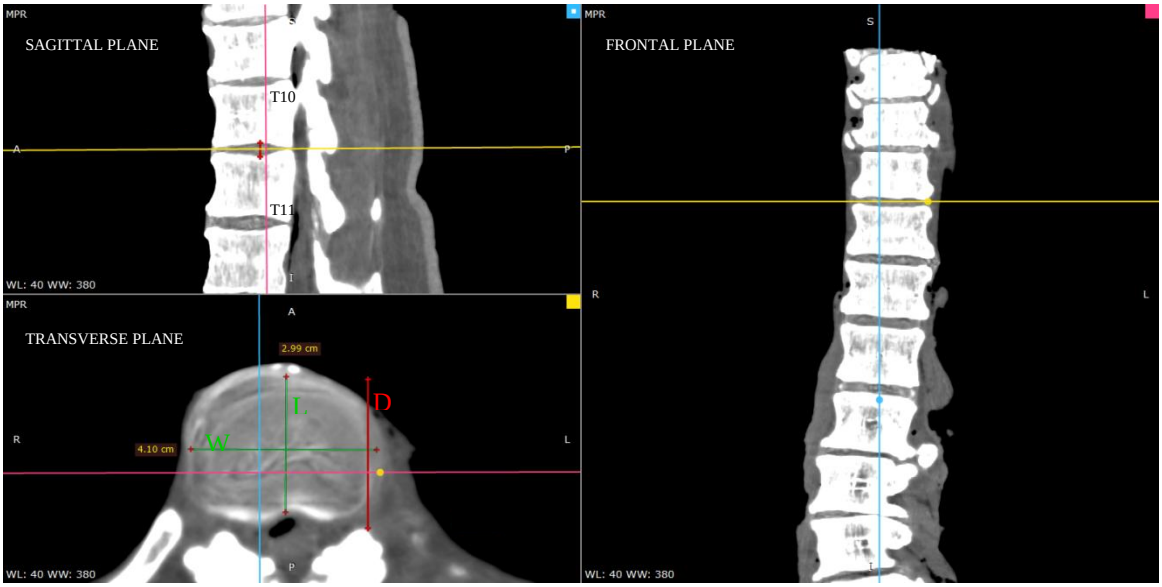

Figure 2.14– *RadiAnt DICOM viewer interface. In the sagittal planele yellow line marks the midplane of the disc. In the transverse plane the green lines represent the disc length (L) and the disc width (W), the red lines is the distance D.*

2.2 Mechanical tests

2.2.1 Testing set-up

In order to see how the disc defects impact the biomechanics of the spine, all the specimens were tested on an uniaxial servo-hydraulic testing machine (8032, Instron, UK), equipped with a 100kN load cell.

Tests were conducted applying a pre-defined load scaled (scaled for each donor body weight). The actuator speed was adjusted for each specimen so that the loading time was the same for all. During the test, each FSU was anchored with the metallic upper pot to the load cell by means of a metallic plate, which had the role to transfer the load between the pot and the load cell with an homogeneous distribution. The lower part of the specimen was linked to the actuator by means a spherical joint, able to move along the antero-posterior direction by means of a low-friction rail. In this way one free rotation of the loading plate was allowed only in the rail direction (*Figure 2.15*).

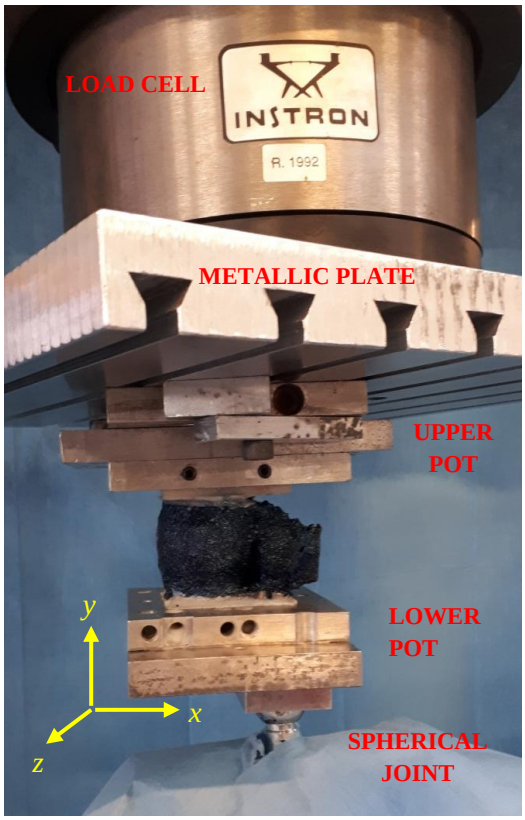

Figure 2.15 *- Testing set up and in yellow the coordinates system.*

2.2.2 Testing protocol

All the specimens were tested in flexion and in extension in all the configurations described above. The position of the specimen under the testing machine was performed taking into account that the spherical joint had to impact the lower pot in its middle right-to-left direction, and that the lateral side with the speckle pattern had to be seen by the cameras.

The tests were sequentially performed and the disc defects were increased with cuts or removing materials after testing both the loading conditions.

The specimens were tested under an axial load applied with an offset. For this combination, a load of 50% of the body weight was applied to be in the range of the in-vivo-load [x] (*Table 2.5*).

Sp. N°	Level	Load (N)	Flexion offset [35%*L*](cm)	Extension offset [70%*L*](cm)
#1	T9 - T10	211	0,85	1,70
#2	T11 - T12	211	0,93	1,86
#3	T10 - T11	402	1,05	2,1
#4	L4 - L5	388	1,73	3,46
#5	T12 - L1	402	1,17	2,34
#6	T10 - T11	495	1,31	2,62
#7	T12 - L1	495	1,34	2,68
#8	T10 - T11	~~647~~ *300*	0,82	1,64

Table 2.5 *- Testing parameters: load and offset values for flexion and extension.*

The estimated load of 647N for the #8 FSU was too high with regard to the size of the specimen, so, to avoid to damage the specimen, it has been decided to reach only 300N, after having non destructively check that the specimen was able to reach this. To be sure to reach the target load during the tests, a 10% increased load was applied.

Being in displacement control, the displacement needed to reach the targeted load was measured and then applied for the tests.

Specimens were solicited with the same load either in flexion either in extension, but the points of application of the load were different (*Table 2.5*). In particular, in flexion tests the load was applied with an anterior offset of 35% of the antero-posterior disc length from the center of the IVD; while, the extension offset were 70% of the antero-posterior disc length (*Figure 2.16*).

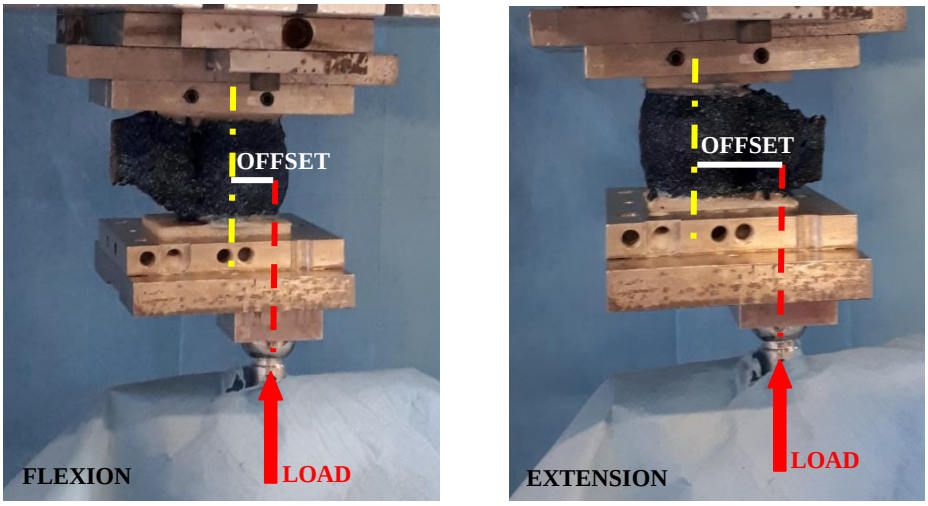

Figure 2.16 *- White lines represent the applied offsets between the center of the disc and load in flexion (left) and extension (right).*

Before starting the tests preconditioning was performed to minimize viscoelastic creep effect, applying a sinusoidal loading at 0.5 Hz for 20 cycles, and it was repeated every time the loading condition was changed.

Each test consisted of six cycles of a trapezoidal wave. The amplitude of the wave was determined previously to the test by reaching manually the targeted load and recording the corresponding displacement. The loading curve lasted 1 second; le load was maintained for 0.3 second; le unloading curve lasted 0.5 second and after 0.2 second a new wave started.

This test was repeated five times for each different loading condition and configuration.

Each test was repeated after 3 minutes from the previous one because it was found to be a time needed to recover the properties of the disc (*Figure 2.17*).

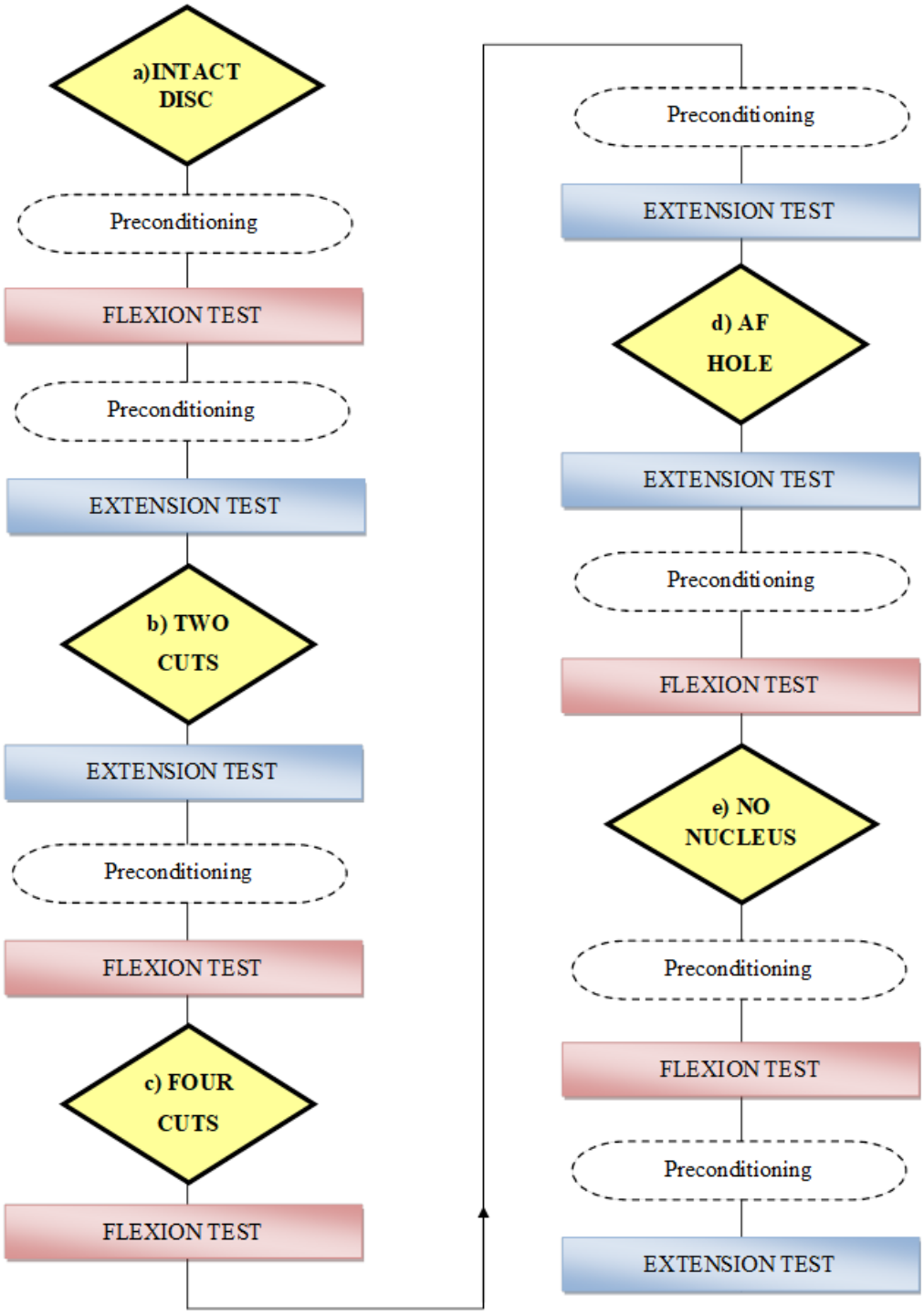

***Figure 2.17** – Block diagram of the testing protocol.*

2.2.3 Data acquisition

During the test, the load and the displacement of the actuator were recorded by the PXI system. at 500 Hz.

Disc surface images were recorded by a 3D-DIC system (Q400, Dantec Dynamics, Denmark) at 15 Hz. The whole system consisted of:

- Two monochromatic cameras (5 MegaPixels, 2440 x 2050 pixels, 8-bit) equipped with standard 35 mm lenses (Apo-Xenoplan 1.8/35, Schneider-Kreuznach, Bad-Kreuznac, Germany) for a stereo-scopic view (*Figure 2.18*);
- Data acquisition card (It manages to import images recorded by the cameras, and to connect, at the same time it records images, others measurement tools with the digital signal output);
- Source of light (two white LEDs, were used) (*Figure 2.18*);
- Computer with the associated DIC software for the images correlation and elaboration;
- Calibration target (Mod. A14-BMB- 9x9, Dantec Dynamics).

The optimized parameters [Ruspi *et al., 2018*] used for the images correlations were:

- Facet Size: 35 pixel;
- Grid Spacing: 19 pixel.

All images were filtered using *Contour* and *Displacement Smoothing*, filters with a *local regression* with a 07x07 kernel size.

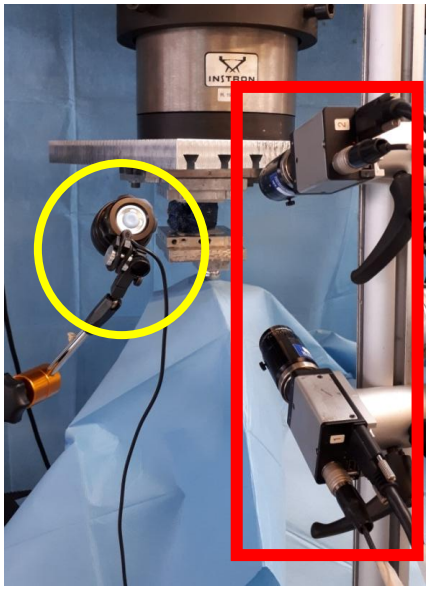

Figure 2.18 - *DIC set up with the two cameras (red square) and the source of light (yellow circle).*

2.3 Data Analysis

Analyzed data were extracted from the last cycle of each test, the first five cycles ensuring that the visco-elastic effect was negligible in the specimens. Indeed, it was confirmed that after three cycles, specimens reached an equilibrium.
Data-processing was performed with Matlab (Mathworks, Inc., Natick, Ma, Usa) dedicated scripts.
Images analysis was performed with the associated DIC software after that the images correlations were successfully performed using optimized parameters described above. Images processing was performed at the target load frame.

The load – displacement curves were obtained from the PXI data to evaluate the loading curve trend between the different configurations. Stiffness was defined as the average slope of the second half of the loading phase.

ROM was defined as the relative rotation between the two vertebral bodies in the sagittal plane at the peak load. In order to obtain the ROM, the following steps were performed on a Matlab scrip, assuming rigid body motion.
For each test:

- The load signal was filtered with a median filter;
- The signal was segmented into the six cycles of the test;
- The peak load, the targeted load and their time interval were computed for each cycle, since to be sure to reach the target load, a targeted load more 10% was applied;
- On the DIC correlated images, two regions of interest were selected corresponding to the upper fixed vertebral body and the lower moving one;
- The position of the center of the each vertebra was plotted was plotted in order to identify the peak load and the unload frame for each cycle of the test;
- Combining the time gap between the target load and the peak load, with the load peak frame allowed to identify the targeted load frame number;
- Distance between the unload frame and the peak value frame were computed for both the centers of the lower vertebra and of the upper vertebra;

- Considering vertebrae as rigid bodies, Singular Value Decomposition Algorithm [Chung et Teoh, 2002] was applied to take out the main rotation and;
- The 3D rotations of the FSU resulted by the composition of the upper and lower vertebra rotation.

In order to assess how strain distribution changed in the different tested configurations, strain distribution maps were extracted over all the correlated surfaces, either for the maximum principal strains either for the minimum principal strains, at the targeted load frame. In addition, the mean, the maximum and the minimum value for the principal strains on the disc surfaces were extracted using the DIC software.

In order to assess changes in disc height under load and due to disc lesions, the disc height was measured on DIC correlated images following the 3D profile to recognize the disc geometry. The disc height was measured in the central lateral side, at the beginning (10N) of the last cycle, to have a comparable measures for all the specimens. The disc height measure in the postero-lateral of the IVD at the peak load was not always possible due to defects in the correlated images.

To limit the inter-specimen variability influence, stiffness, height and ROM values were normalized to the intact condition value. Median of all the outcomes were calculated and presented.
For each outcome, outliers checked and excluded using Peirce's criterion [Ross, *2003*].

2.4 Statistical Analysis

A statistical analysis was performed to evaluate the significance of the changes between the disc damage conditions.
The median stiffness and ROM, both in flexion and in extension, were compared using the *Friedman One-Way Repeated Measure Analysis of Variance by ranks*. *Friedman*'s test is a-non parametric statistical test for paired data used to detect differences in treatments across multiple test attempts.
A statistical significance of 0.05 was used for all statistical tests. A *p-value* smaller than 0.05 was considered statistically significant.

Chapter 3

Results

All the tests were successfully implemented without damaging the specimens.
Correlations and measurements were successfully performed for all the different configurations of all specimens.

3.1 Stiffness

For each specimen and for each type of motion, load – displacement curves were compared in the five conditions. Displacement offset was removed to have the curves starting at zero displacement. Being interested in the loading condition, only the loading phases until the targeted load were plotted.

Different behaviors were observed through the load – displacement curves were observed in the flexion condition: six specimens showed an increase of slope between configuration a) and d) (*Figure 3.1*), while the other two specimens (#4 and #6) exhibited the opposite tendency (*Figure 3.*2) The nucleotomy curves showed an effect more intense than the others in all the spine, except in one specimen.

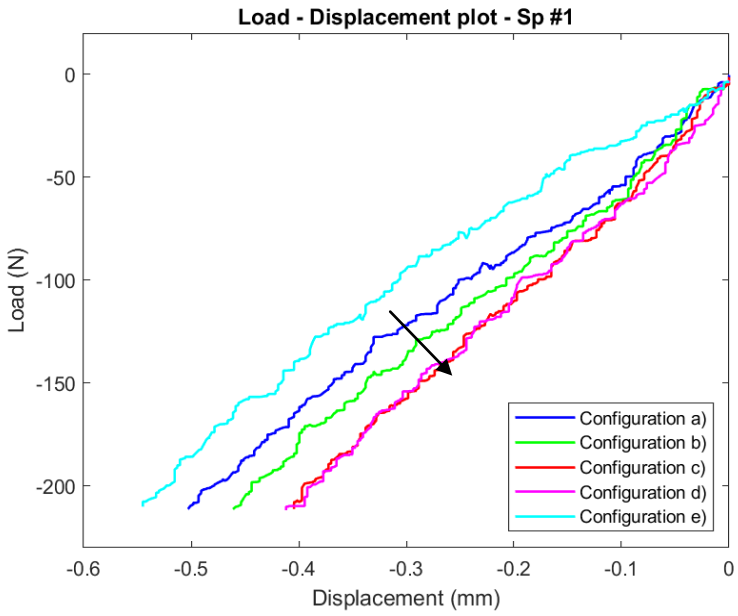

Figure 3.1 - *Load – displacement plot with a slope increasing between configuration a) and d), in flexion.*

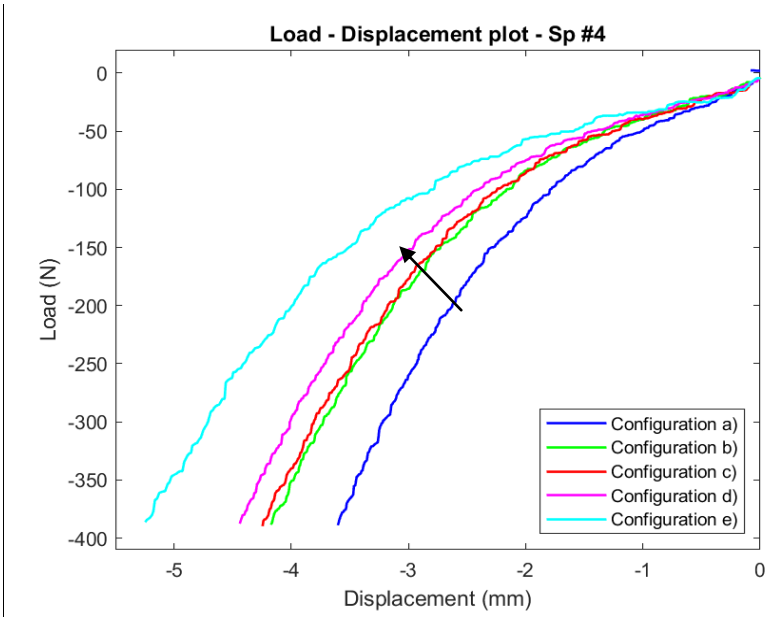

Figure 3.2 - *Load – displacement plot with a slope decreasing between configuration a) and d), in flexion.*

In addition, the FSU's belonging to the upper part of the spine (between T9 and T11) presented a linear shape (*Figure 3.1*) whereas the lower part of the spine (between T12 and L5) showed an exponential shape (*Figure 3.2*).

A common trend among the specimens was the increase of the *sigmoid-shape* curve in the laxity zone (first part of the curve): usually the first curve (blue one, condition a)) was linear. Increasing the incision level, this effect was more stressed until the nucleotomy step (light blue curve, configuration e)) (*Figure 3.3*).

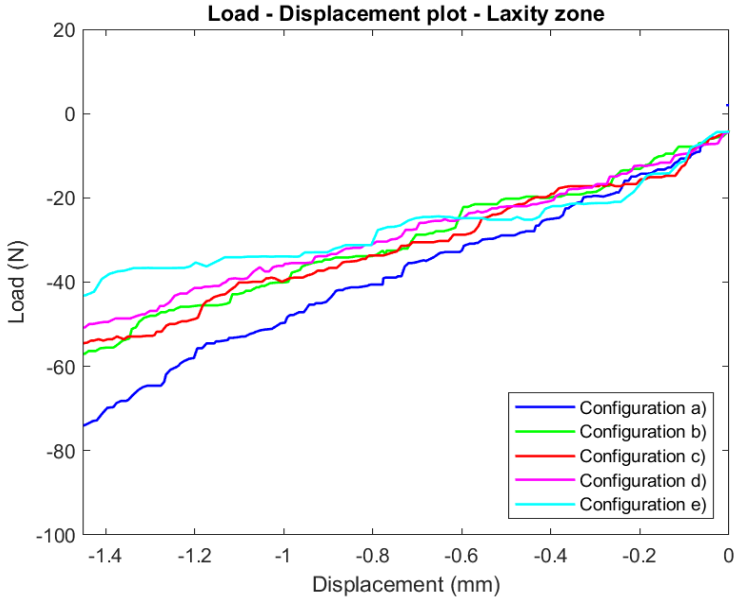

Figure 3.3 - *Zoom on the initial load-displacement plot; the sigmoid-shape effect increase is visible from the blue line (conf. a)) to the last defect simulation (light blue line).*

In extension, load and displacement were linearly related, except for the lumbar FSU #4 which exhibited an exponential behavior (*Figure 3.4*). As in flexion, half of the specimens showed an increase of slope between configurations a) and d), while the others half exhibited the opposite tendency. In addition nucleotomy condition exhibited an effect more intense or comparable to the others, except for FSU #5, which manifested a sharp increase of the load – displacement slope after nucleus removal (*Figure 3.5*).

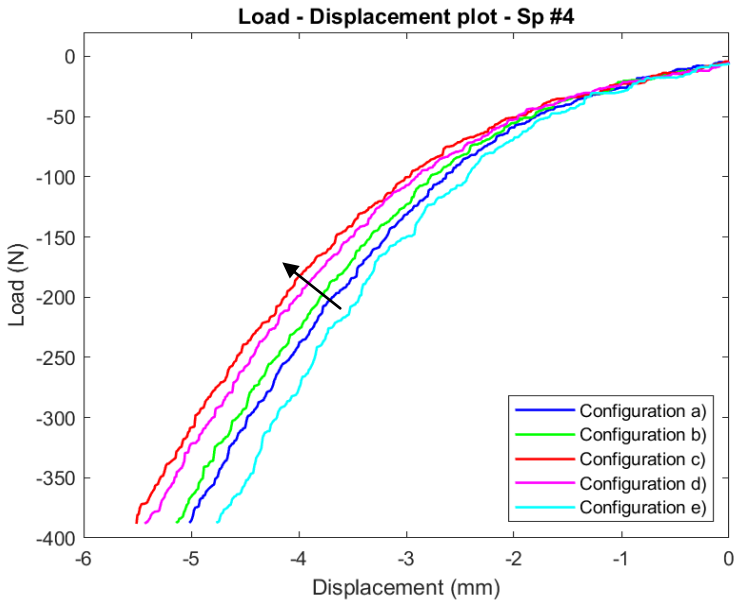

Figure 3.4 – *Load – displacement curves with a slope decreasing between configuration a) and d) in extension. Nucleotomy curve has a comparable effect to the others. All the curve show an exponential behavior.*

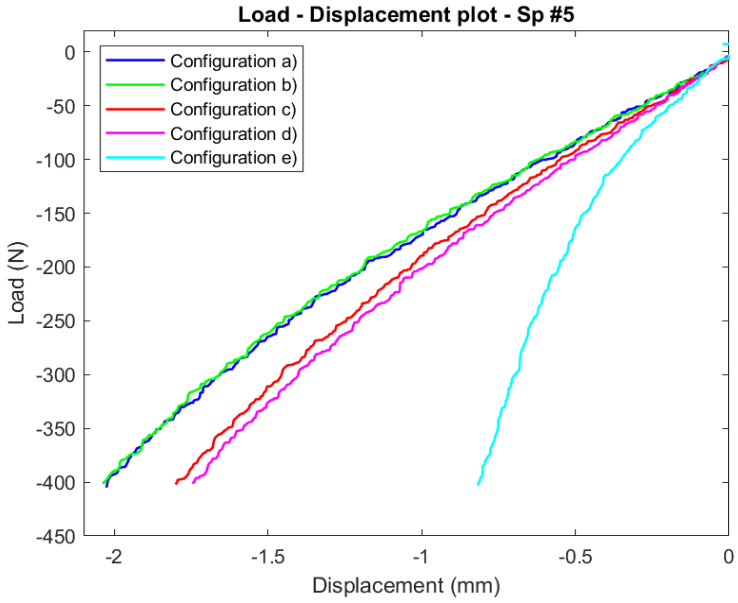

Figure 3.5 – *Load – displacement curves with a linear behavior in extension. Sharp increase of slope in nucleotomy condition (light blue curve).*

Due to these different trends of the loading curves, in order to have a comparable parameter between the specimens, stiffness was estimated as the slope of the second half of the loading curve, which was more consistent for all specimens.
The median values of the stiffness normalized by intact state of the last cycle of the five repetitions are presented.
Deleted data on tables were classified as outliers according to Pierce's criterion [Ross, *2003*] and therefore they were excluded from analysis and plot.

In flexion, specimens presented very different trends among the various configurations (*Table 3.1*) but the dispersion of the values was comparable between the increasing disc lesions (*Figure 3.6*).

	CRANIAL <==					==> CAUDAL			
Sp. N°	**#1**	**#3**	**#6**	**#8**	**#2**	**#5**	**#7**	**#4**	***Median***
Level	*T9 - T10*	*T10 - T11*	*T10 - T11*	*T10 - T11*	*T11 - T12*	*T12 - L1*	*T12 - L1*	*L4 - L5*	
Conf. a)	1,00	1,00	1,00	1,00	1,00	1,00	1,00	1,00	*1,00*
Conf. b)	0,98	1,01	1,02	1,13	0,95	1,04	1,00	0,91	*1,00*
Conf. c)	1,01	0,96	1,03	1,16	1,02	1,06	1,02	0,87	*1,02*
Conf. d)	1,05	0,88	1,01	1,27	1,06	1,08	1,15	0,89	*1,05*
Conf. e)	1,01	0,96	0,95	1,13	0,78	1,20	~~1,58~~	0,76	*0,98*

Table 3.1 *- Median stiffness values in flexion. Results have been sorted by levels.*

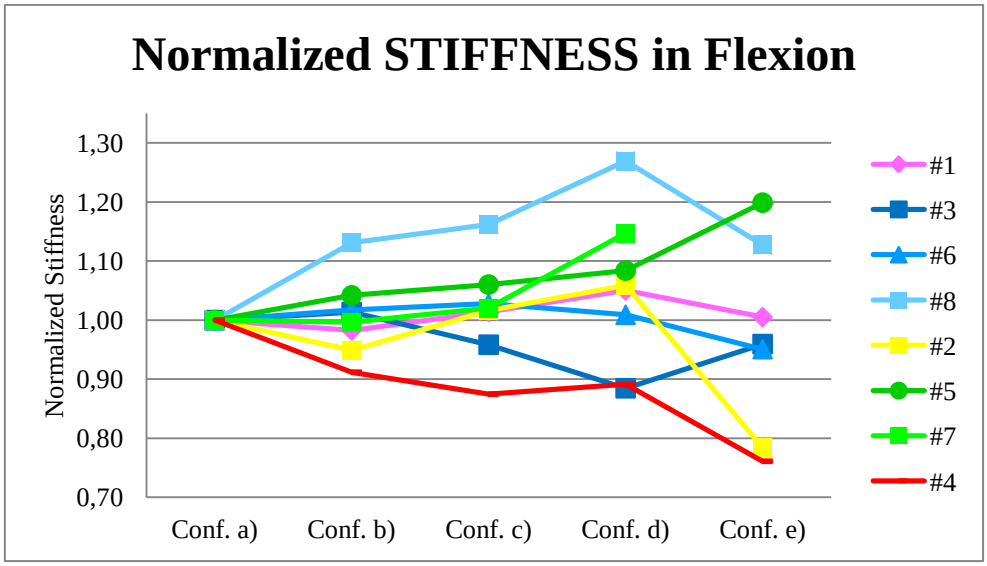

Figure 3.6 *- Normalized stiffness trend in flexion for each specimen in relation to the increasing degree of disc damage from configuration a) (intact) to e) (complete nucleotomy).*

Median values of all the specimens, were very similar between damage levels (*Figure 3.7*). Configuration without nucleus (e) showed a little decrease in the median value of stiffness, but the minimal differences between the configurations were not statistically significant, with $p = 0.86$ (Friedman test).

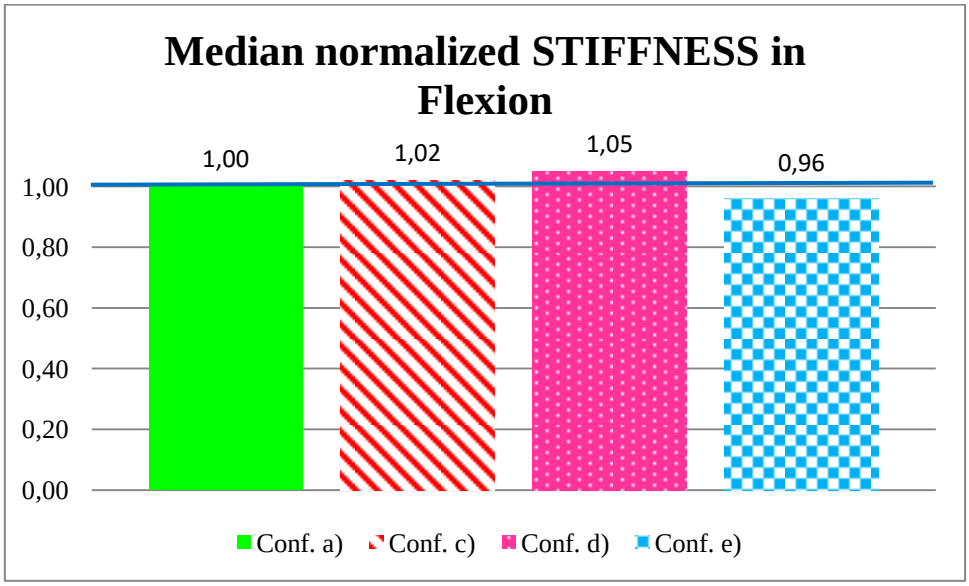

Figure 3.7 - *Median normalized stiffness in flexion for each configuration; from configuration b) (two incisions) to e) (complete nucleotomy). The blue line represents the intact disc stiffness level.*

In extension (*Table 3.2*), two vertical cuts (configuration b)) seemed not to have any effect on the stiffness of the specimens.

From 4 cuts (configuration c)), the specimens showed a larger variability, with a variation of stiffness between 40% reduction and 20% increase. Configuration c) and d) had similar stiffness for all specimens. Nucleus removal enhanced inter-specimen variability with a decreasing stiffness for half of the specimens and an increasing stiffness for the others (*Figure 3.8*).

	CRANIAL <==					==> CAUDAL			
Sp. N°	**#1**	**#3**	**#6**	**#8**	**#2**	**#5**	**#7**	**#4**	***Median***
Level	*T9 - T10*	*T10 - T11*	*T10 - T11*	*T10 - T11*	*T11 - T12*	*T12 - L1*	*T12 - L1*	*L4 - L5*	
Conf. a)	1,00	1,00	1,00	1,00	1,00	1,00	1,00	1,00	*1,00*
Conf. b)	1,08	1,01	0,99	1,05	1,01	0,98	1,09	1,02	*1,02*
Conf. c)	0,61	1,15	0,87	1,17	1,11	1,09	1,29	0,99	*1,10*
Conf. d)	0,62	1,14	0,88	1,22	1,14	1,12	1,44	0,96	*1,13*
Conf. e)	0,54	1,33	0,88	0,88	0,79	~~3,18~~	1,53	1,11	*0,88*

Table 3.2 - *Median stiffness values in extension. Results have been sorted by levels.*

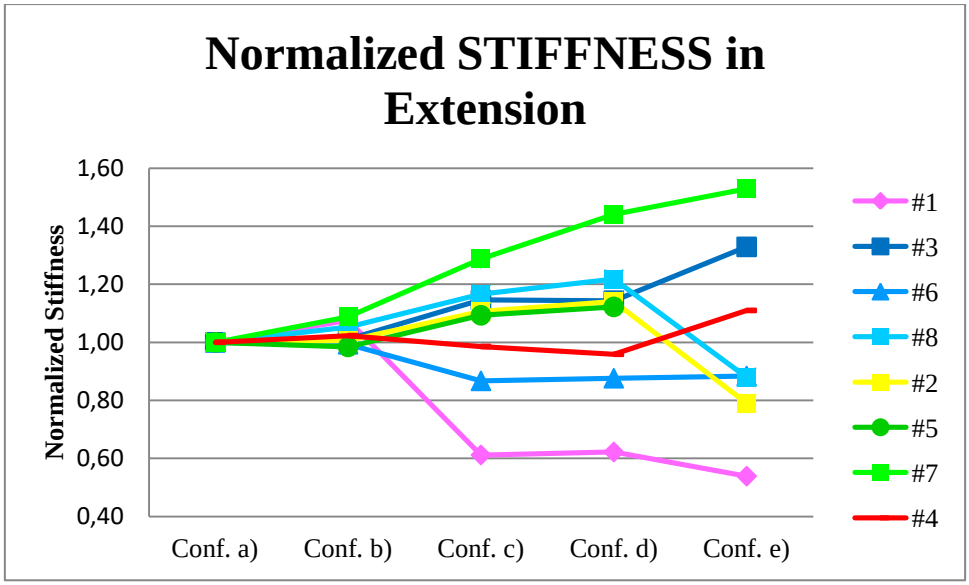

Figure 3.8 - *Normalized stiffness trend in extension for each specimen in relation to the increasing degree of disc damage from configuration a) (intact) to e) (complete nucleotomy).*

Applying defects b) and d) did not affect significantly the stiffness median values (*Figure 3.9*) with respect to the cases a) and c). An increment of 10% was obtained after the four cuts (configuration c)), while decrease of 12% occurred after nucleus removal with respect to the intact state.

Different configurations did not show statistically significant differences ($p = 0.71$, *Friedman test*).

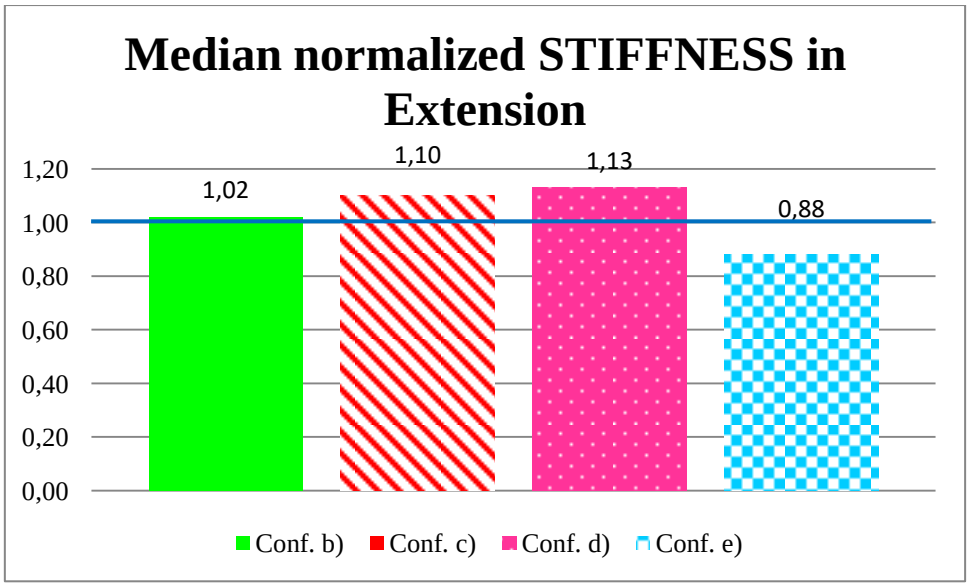

Figure 3.9 - *Median normalized stiffness in flexion for each configuration; from configuration b) (two incisions) to e) (complete nucleotomy).*
The blue line represents the intact disc stiffness level.

3.2 Range of Motion

Only motion in the sagittal direction was taken into account.

For each configuration, the median of the ROM of all specimens were normalized by the intact ROM for each motion.

Deleted data on tables were classified as outliers according to Pierce's criterion [Ross, *2003*] and therefore they were excluded from analysis and plot.

In flexion, two vertical cuts (configuration b)) resulted in an increase of the ROM for all specimens except two (*Table 3.3*).

	CRANIAL <==					==> CAUDAL			
Sp. N°	**#1**	**#3**	**#6**	**#8**	**#2**	**#5**	**#7**	**#4**	***Median***
Level	*T9 - T10*	*T10 - T11*	*T10 - T11*	*T10 - T11*	*T11 - T12*	*T12 - L1*	*T12 - L1*	*L4 - L5*	
Conf. a)	1,00	1,00	1,00	1,00	1,00	1,00	1,00	1,00	*1,00*
Conf. b)	1,23	1,43	1,48	0,67	1,03	1,07	0,71	1,09	*1,08*
Conf. c)	1,22	1,28	1,26	0,62	0,91	1,05	0,79	1,12	*1,09*
Conf. d)	1,19	1,17	1,50	0,62	0,73	0,97	0,90	1,26	*1,07*
Conf. e)	1,03	0,86	0,81	~~1,50~~	0,85	0,70	0,63	1,13	*0,85*

Table 3.3 - *Median ROM values in flexion. Results have been sorted by levels.*

Between the configuration b) and d), no clear common trend was observed in the specimens but the ROM values remained in a range of [60%; 150%] for these three configurations. Nucleus removal decreased the ROM compared to the previous configurations, except in FSU #2; for the majority of the specimens the ROM was lower than the intact configuration value (*Figure 3.10*).

Differences between all the configurations were found to be not statistically significant, with $p = 0.20$.

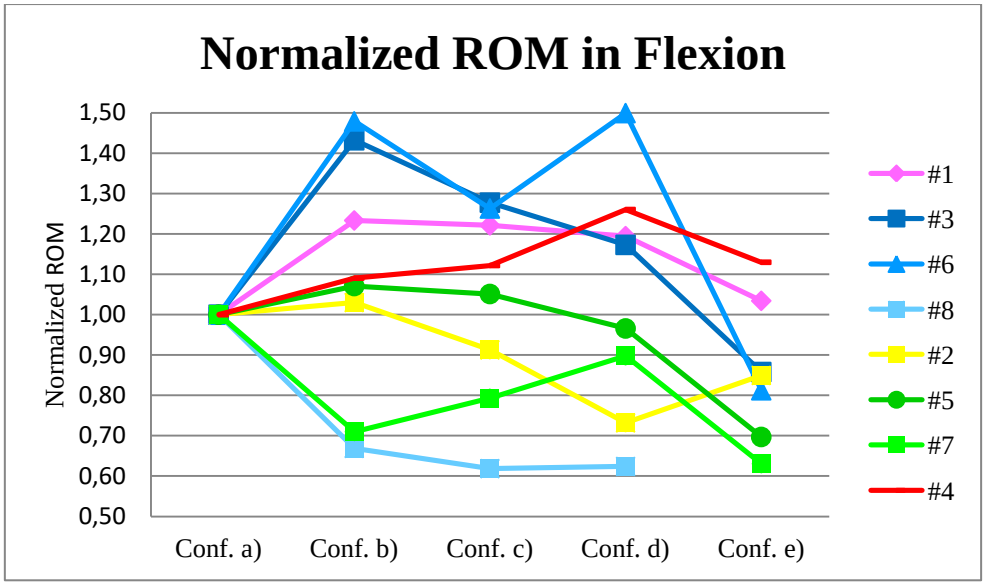

Figure 3.10 -- *Normalized ROM trend in flexion for each specimen in relation to the increasing degree of disc damage from configuration a) (intact) to e) (complete nucleotomy).*

Looking at the median values among all the specimens (*Figure 3.11*), the disc lesions effect resulted in an increase of the rotation between 7% and 9% configurations b), c) and d), compared to the intact case. A 15% ROM decrease was achieved in the nucleotomy state (e)).

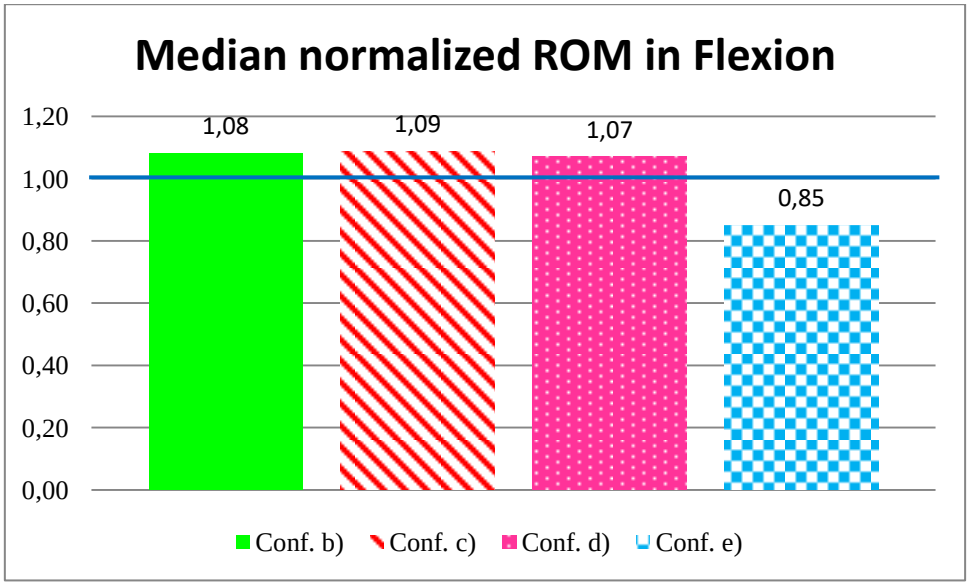

Figure 3.11 - *Median normalized ROM in flexion for each configuration; from configuration b) (two incisions) to e) (complete nucleotomy).The blue line represents the intact disc ROM level.*

In extension, specimen #1 was excluded after the ROMs in configuration c), d) and e) were found to be outliers with values three times higher than the other specimens (*Table 3.4*).

	CRANIAL <==					==> CAUDAL			
Sp. N°	**#1**	**#3**	**#6**	**#8**	**#2**	**#5**	**#7**	**#4**	***Median***
Level	*T9 - T10*	*T10 - T11*	*T10 - T11*	*T10 - T11*	*T11 - T12*	*T12 - L1*	*T12 - L1*	*L4 - L5*	
Conf. a)	~~1,00~~	1,00	1,00	1,00	1,00	1,00	1,00	1,00	*1,00*
Conf. b)	~~0,94~~	0,99	1,01	0,93	1,23	1,06	0,80	0,92	*0,99*
Conf. c)	~~2,70~~	0,77	1,49	0,72	0,93	0,95	0,85	0,89	*0,89*
Conf. d)	~~1,97~~	0,77	1,38	0,66	1,11	0,90	0,80	0,88	*0,88*
Conf. e)	~~4,01~~	0,49	1,03	0,95	1,50	0,26	0,67	0,84	*0,84*

Table 3.4 *- Median ROM values in extension. Results have been sorted by levels.*

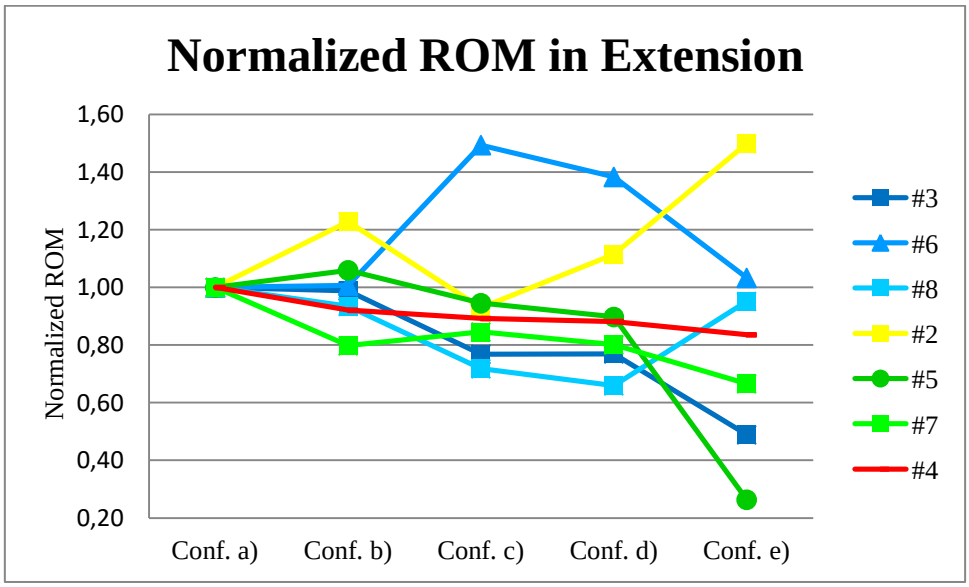

Figure 3.12- *Normalized ROM trend in extension for each specimen in relation to the increasing degree of disc damage from configuration a) (intact) to e) (complete nucleotomy).*

Similarly to flexion, different behaviors between the specimens were observed in extension, in particular FSU #2 and #6 showed a completely different behavior from the other specimens (*Figure 3.12*). The majority of FSUs showed the same relative rotation between vertebral bodies after the first two cuts compared to the intact segment.

Except few cases, a ROM reduction was noticed in configuration c) and e), compared with the step before them (b) and d)). Furthermore, the final values were inferior to the

intact case. After removing the annulus square, no remarkable variations were visible in relation to the previous configurations.

The median values among the specimen revealed no changes in ROM after the first lesion confirming the previous observations (*Figure 3.13*).

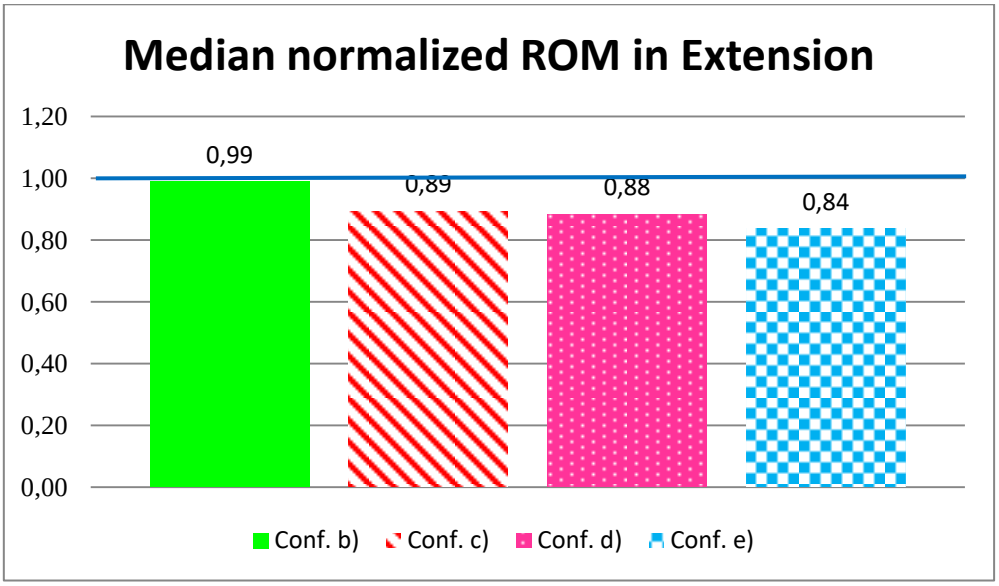

Figure 3.13 *- Median normalized ROM in extension for each configuration; from configuration b) (two incisions) to e) (complete nucleotomy).*
The blue line represents the intact disc ROM level.

There was no statistically significant difference between the five configurations although a prevalent trend of range of motion decreasing was observed ($p = 0.48$, *Friedman test*).

3.3 Strain distribution

DIC correlation has been successfully performed for all tests in flexion and extension.
Both in flexion (*Figure 3.14*) and in extension (*Figure 3.15*), the highest strain values were located in the disc while the vertebra underwent null strain.

In flexion, tensile principal strains were found in the center of disc. From a) up to d), the annulus surface was entirely strained, but in configuration e) the strained region concentrated along the mid-height plan of the disc. Strains direction showed that maximum tensile strains were circumferentially aligned in flexion. Compressive strains showed two different trends depending on the specimen level (*Figure 3.16*). In thoracic segments, high compressive strain values were located along the endplates starting from the anterior part (a)), propagated back along the endplates until the center of the lateral side of the disc. With the increasing damage, strains migrated and concentrated at the cranial and caudal borders, ending by covering the entire disc surface in the anterior (e)). In lumbar levels, segments with a small defect showed high compressive strains in the anterior ligament and along the endplates. The damages reduced the strains in the ligament, concentrating the high values along the endplate, propagating to posterior part of the disc.

In extension, thoracic and lumbar levels acted differently (*Figure 3.17*). In thoracic levels, tensile strains spread incrementally on the disc from localized high strain regions on intact thoracic discs to continuous distribution over the disc in e). In lumbar segments, not only the disc was strained but also the anterior ligament leading to high tensile strains covering the anterior part of vertebrae. Contrary to thoracic levels, the strain distribution reduced when the disc got more damaged, with a concentration of the strain on the disc only. Tensile strains presented an axial alignment for all spine levels. Compressive strained regions were observed at the posterior part of the disc. In thoracic segments, the strains extended to the anterior of the disc with the damage increase whereas in lumbar segment, the distribution reduced incrementally, and concentrated around the endplates after nucleotomy.

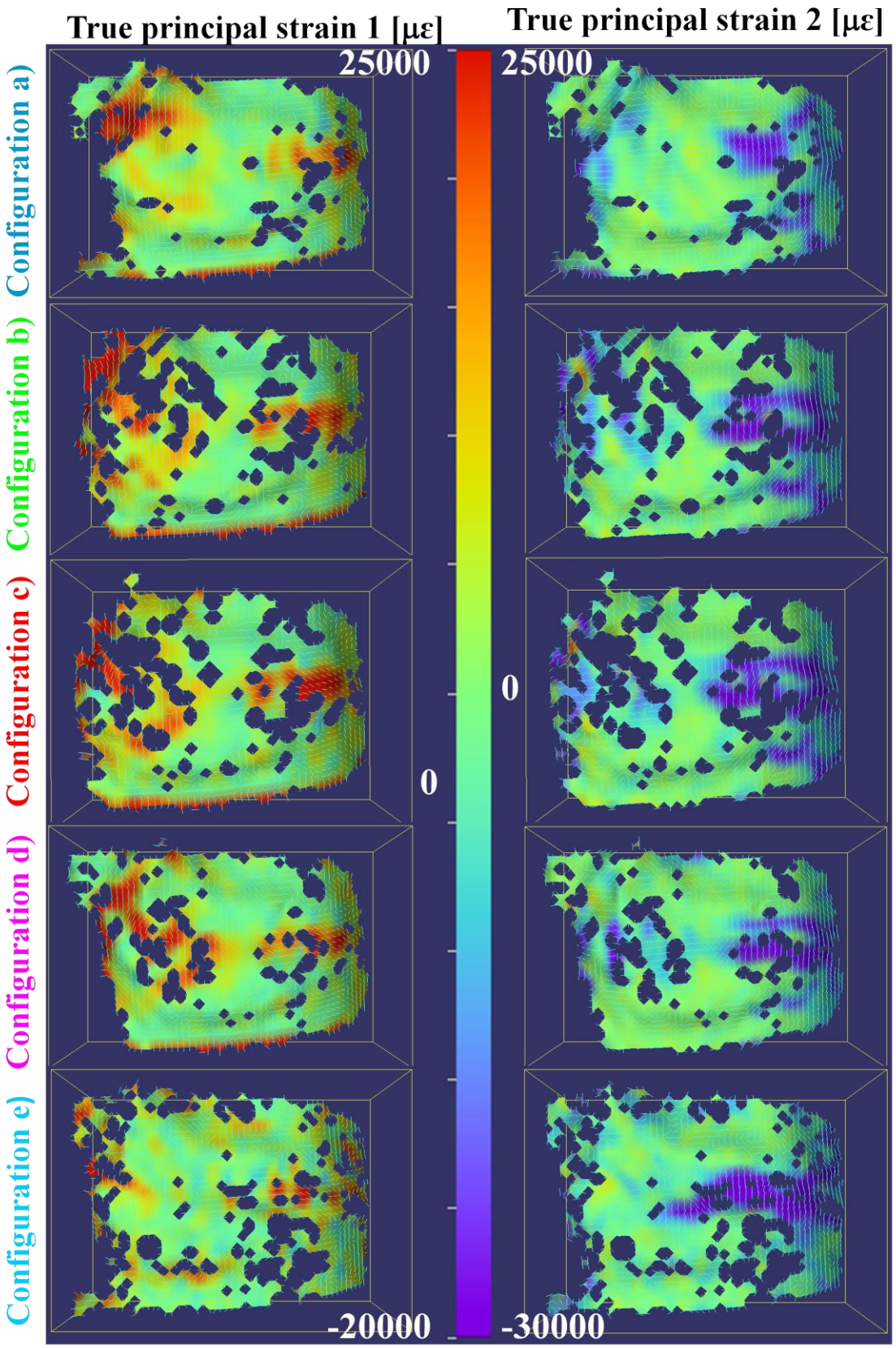

Figure 3.14 –
True principal strains in FLEXION, between configuration a) and e).

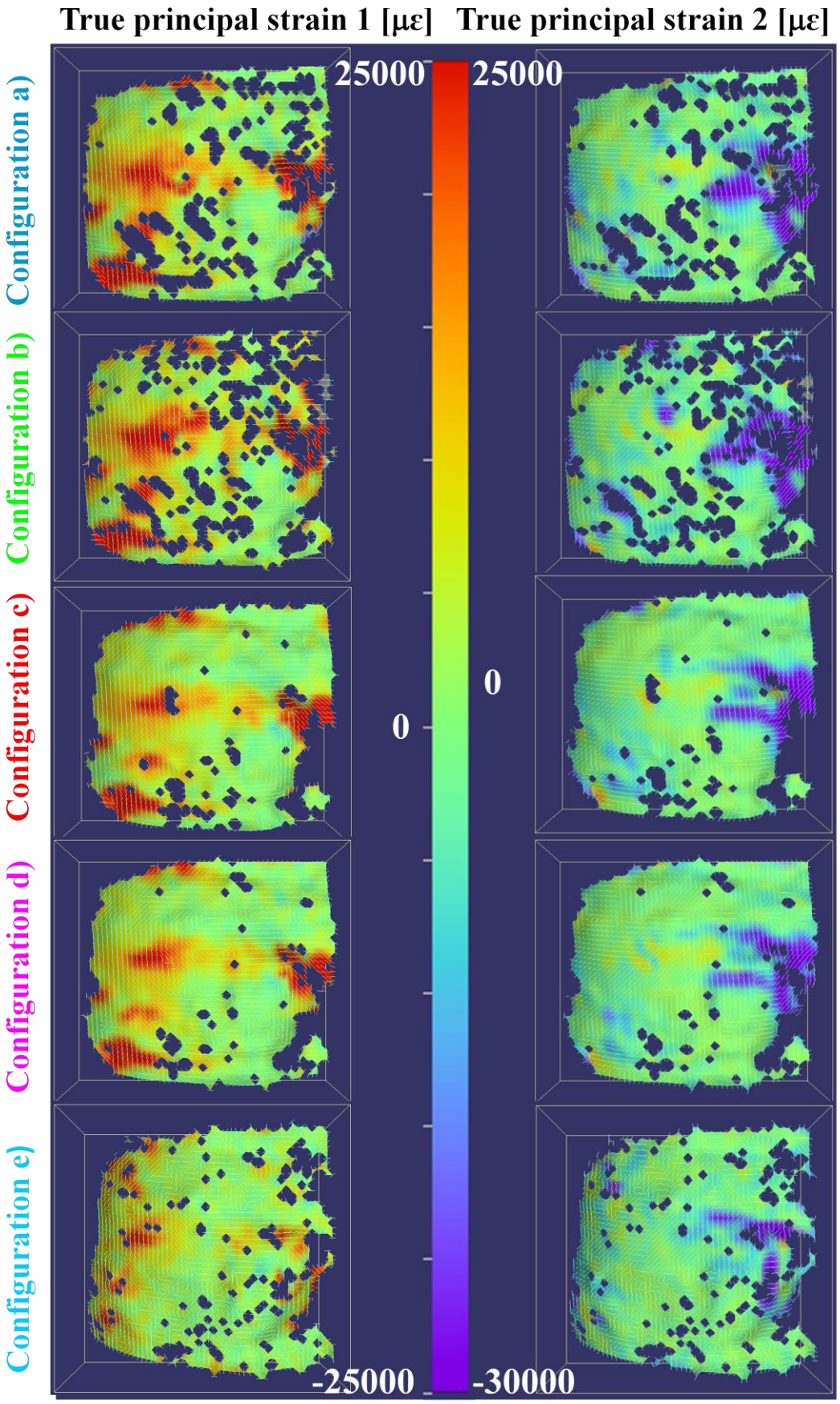

Figure 3.15 –
True principal strains in EXTENSION, between configuration a) and e).

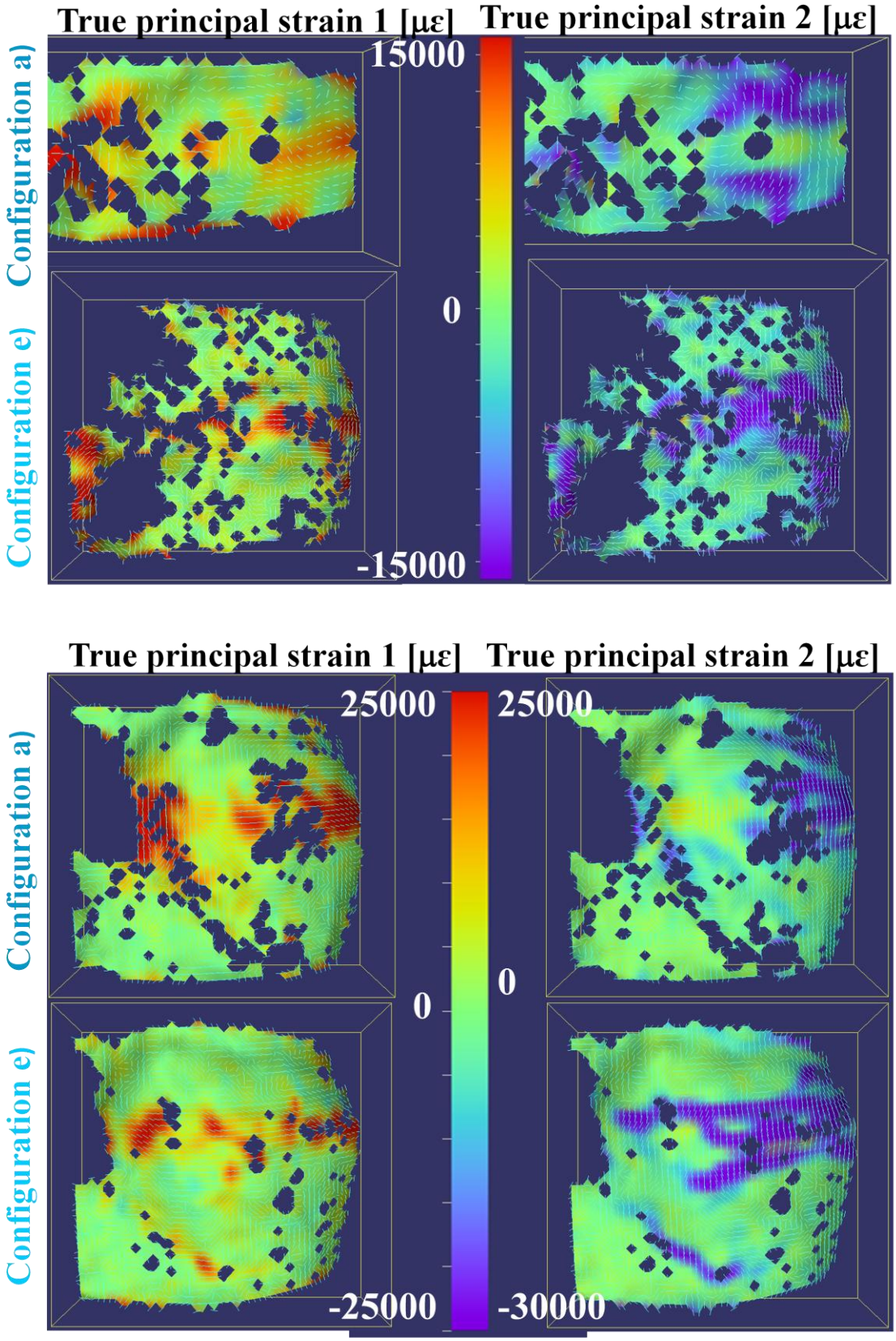

Figure 3.16 –
True principal strains in FLEXION, in configuration a) and e)
in a thoracic segment (up) and in a lumbar segment (down).

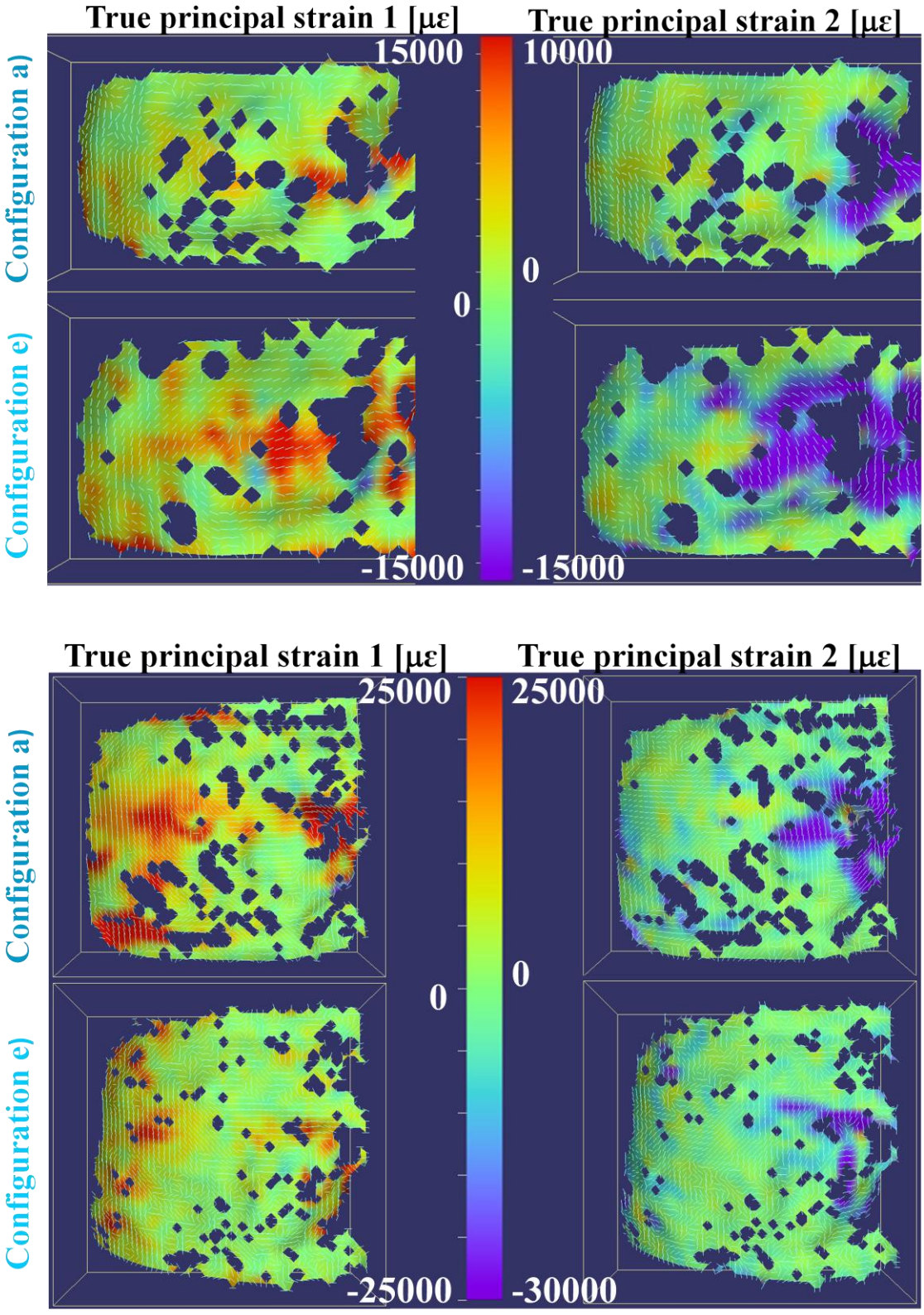

Figure 3.17 –
True principal strains in EXTENSION, in configuration a) and e) in a thoracic segment (up) and in a lumbar segment (down).

Median values of average, minimum and maximum values of true principal strain are shown in *Table 3.5*. Because of the inter-specimen variability, details for each specimen are in Appendix A.

Nucleotomy affected more compressive strains either for flexion either for extension, than tensile strains. No configuration showed peak of tensile strains values significantly higher compared to the other configurations whereas compressive strain values doubled for d) and e) compared to intact condition.

ε_1	FLEXION		EXTENSION	
	Mean [με]	Max [με]	Mean [με]	Max [με]
a)	8550	45770	5150	40258
b)	8800	41001	6850	39145
c)	9550	43199	5700	50241
d)	9500	44281	6060	55377
e)	8000	47199	5150	48034

ε_2	FLEXION		EXTENSION	
	Mean [με]	Min [με]	Mean [με]	Min [με]
a)	-7000	-42690	-4755	-61289
b)	-5650	-55972	-4400	-74290
c)	-10000	-60316	-3500	-86160
d)	-10900	-85611	-4850	-100874
e)	-30000	-115889	-8700	-95802

Table 3.5*- Median values of average, minimum and maximum first (Ɛ1) and second (Ɛ2) principal strains over the disc surface for flexion and extension.*

3.4 Disc height

Disc heights were measured for each test and normalized to the initial disc condition for each specimen.

Only after the nucleus removal an appreciate decrease in the disc height was observed.

Table 3.6 shows the median percentage of disc height loss in each configuration, compared to the intact state.

Disc height loss

	Conf. b)	Conf. c)	Conf. d)	Conf. e)
Flexion	0,5%	0,8%	2,3%	23,0%
Extension	0,2%	1,3%	1,9%	20,3%

Table 3.6 *– Disc height loss. Median values in percentage of all specimens.*

Chapter 4

Discussion

The main aim of this study was to assess the mechanical stability and strains distribution on thoraco-lumbar FSUs following disc defects. FSUs were tested sequentially in flexion and extension with five disc lesions, starting from intact condition to the nucleus removal.

The sequentially execution of disc damage did not significantly impact the spine biomechanics in terms of stiffness and range of motion: no statistical differences were observed for these outcomes.

The intervertebral disc height was not affected by annulus damages between configuration a) and d), but IVD decreased after nucleus removal, confirming the clinical observations (Varga *et al. 2015*).
Furthermore, some specimens, corresponding to those with the maximum disc height reduction due to nucleotomy, showed during the last flexion test an inward bulging of the annulus. A possible explanation is that because the hydrostatic pressure of the nucleus pushes the annulus outward under compressive loading the absence of nucleus results in the abnormal bulging, [Seroussi *et al, 1989*]. Finally, although the continuity of the annulus was interrupted in the postero-lateral side, no leakage of the nucleus was observed.

The normalized values of stiffness did not show any statistical difference among the different configurations in flexion because of the different specimens presented very different trends. In particular, median values between configuration b) and c) did not revealed differences but looking at each specimen individually, almost all of them presented an increment in stiffness.
In extension, stiffness in configuration a) and b) and in configuration c) and d) were similar attesting that vertical incision did not disturb the disc stability whereas a squared

cut made the segment stiffer. Nucleus removal affected the segment stiffness, with a drop of the mechanical properties. Alterations in the annulus, like radial and circumferential tears, and nucleus removal, did not impact the linear part of the load – displacement plot, but had a more visible impact on the laxity zone. Depending on the disc damage the first part of the curve showed two macroscopic effects:

- A different slope which reflected le increasing or decreasing trend among the configuration (*Figure 3.1 and 3.2*);
- A significant changing from a linear trend to a *sigmoid shape* increasing the defects (*Figure 3.3*).

Indeed, the changes occurring in the laxity zone due to the damages were more visible in flexion. This is explained by the anatomical function of the facets. In unloaded condition, facets are in contact. In extension, the facets are instantly loaded and so a linear trend is visible. In flexion, the facets reply first with a stiff behavior until they separate. Once the contact between the facet stopped, the load increase stabilizes as long as the facet joints stretch, resulting in an almost horizontal curve. Then, when the facets are enough separated, the posterior ligaments begin to resist the flexion and the stiffness increases again.

Finally, the sharp increase of the nucleotomy curve slope in the extension load-displacement plot of specimen #5 was confirmed by a disc height loss of 28%: the facets came in contact before and it resulted in a stiffer behavior.

In flexion, ROM changes were visible after the first lesion; it created a median ROM increase of 8% compared to the intact state and it remained at the same level for the two subsequent configurations. Thus, the first lesion created the fibers gap responsible for the segment instability. On the contrary, in extension, ROM variation from the intact state was caused by the four cuts.

In both loading conditions, no differences related to the presence or absence of the annulus square plug were observed. It indicates that after the fiber disruption, the nucleus behavior is not affected by the interposed materials.

In extension, a ROM decrease after nucleotomy was hypothesized: the disc height reduction, as a consequence of the nucleus removal, led to a proximity of the facet joints which obstructed the relative rotation between the vertebral bodies. Despite all this, observed differences between the five configurations were no statistically significant.

Generally, both in stiffness and in the range of motion, a large variability in the specimen behaviors was expressed, leading to non significant differences. Such variability could be caused by the spine different levels used and by the nucleus intact condition.

Results showed different strain distributions for thoracic and lumbar segments in flexion and extension.

In flexion, the intact disc is compressed in the anterior part and it is stretched in the posterior one. Emptying the disc, vertebrae collapse on each other while the disc bulges in the frontal part and tensile strains are then located in the mid-height plan of the disc, both for thoracic and lumbar segments. During bulging, compressive strains are located at the endplates junction. Thoracic FSUs present a very small disc. Due to that, height loss of the disc makes the endplates closer, and combined with a small bulging of the disc, the compressive strains located along the endplates cover the entire small disc. On the contrary, in lumbar segments with a higher disc and a more pronounced bulging result in separated compressive strain distributions in the endplates.

In extension, tensile strains are located in the anterior part of the disc and in the intact anterior ligament. The successive damages and in particular the nucleus removal determine the disc fall. In thoracic levels, the anterior ligament is narrow and thin, so the strains on the ligament are distributed over a small area. The disc is small and does bulges in small proportions which results in an incremental stretching of the anterior fibers and increase of tensile. On the contrary, in lumbar segment, larger discs determine a largest void left inside after nucleus removal. This contributes to the vertebrae collapse, associated with a pronounced annulus bulging. Therefore, the tensile strains on the disc decrease because the annulus bugles also in the front. Compressive strains are located in the posterior part of the disc and at the endplates border, when the disc is intact. In thoracic level, in which a small motion is visible, the compressive strains increase after nucleotomy, and spread to the anterior part. The lumbar segments, which bulge more after the nucleus removal than the thoracic levels, show compressive strains located around the endplates.

For all the FSUs, gradual changes in the strain distribution were observed from configuration a) to d), confirming that increasing damages slightly deform the spine tissue. On the contrary, in configuration e), high variation of the strain distribution was

observed with concentration of strains in a located area of the disc or in the endplates which could make the disc more vulnerable to other damages and micro fractures.

To my knowledge very few papers could be found in the literature testing similar defects as this study.

As found in this study, Showalter *et al., 2014*, and Brickmann *et al., 1991*, reported a disc height reduction after nucleotomy.

Stiffness results of the present study are in agreement with the study of Green *et* Adams, *1993;* as they reported that collagen fibers does not need to be continuous to reinforce the annulus and that the fiber-matrix interactions make a large contribution to stiffness. In addition, Michalek *et* Iatridis, concluded in 2012 that, the lack of stiffness change in bending suggests that acute annular tears are not sufficient to induce off-axis motion and instability. On the contrary, large injuries seem to increase the opening of facets and so they resulted in a longer laxity zone [Michalek *et al, 2012*].
Thompson *et al.*, 2000, studying the effect of tear type on biomechanical properties of human lumbar spinal motion segments, found that flexion stiffness increased with more intense severity of concentric tears and rim lesion and extension stiffness increased with increased severity of radial tears.

Stiffness outcomes observed after nucleus removal were different with previous study [Cloyd *et al.*, 2007]. This is possibly due to the fact that, thoracic spine segments which were mainly involved in this study reacted to loading stresses in a different way than the lumbar levels analyzed in literature.
Similarly to this study, Bostelmann *et al.*, 2015, could not detect any significant difference in the flexion and extension range of motion after having created a rectangular window in the annulus. Despite the fact that no significantly difference were exhibited after the nucleus removal compared to the intact state, Kuroki *et al., 2014*, observed that the effects of cyclic loads after nucleotomy increased ROM and caused spinal instability, contrary to this study, where ROM in configuration e) decreased compared to the intact case. Lee *et al.*, 2018, observed similar absolute values in the range of motion of FSUs after nucleotomy, compared to the ones exhibited in this work, but they found differences statistically significant between the intact and the damage disc.

Few studies looked into the strain distribution on the disc surface under the same configuration. Ruspi *et al., 2017* found that different portions of the intervertebral disc were subjected to compression or tension with different orientation of the principal strain. Same was observed in this study: in the compressed side of the disc the compressive strains were axial, while circumferential tensile strains on the stretched side of the disc.

Limitations of the study

The small number of specimen used in this study was responsible for the limited statistical power. Furthermore, the high variability of the levels involved led to different behaviors of the FSUs. However, the results were in accordance with other studies and allowed to draw different trends depending on specimen levels.

Clinically, discoplasty aims at recovering the disc height in order to open the neuroforamen and free the nerve. This surgery is mainly used in lumbar spines so the use of thoracic levels could integrate some bias. However, the results did not show any correlated impact due to the spine level, except for the strain distribution.
In addition, the vertebrae T9 and T10 are biologically linked to the sternum by means of the ribs. This means that these levels undergo a different loading *in vivo* compared to the other vertebrae. The load is also supported in the front and they have a different load transmission related to the lower part of the thoracic spine and to the lumbar segments [Ignasiak *et al*., 2016]. Although ribs were removed in this study, upper thoracic levels could behave differently from others even if no evidence of this was highlighted in this study.

In this study a combination of compression and bending was applied. Indeed this study is related to another work using the same specific setup. Most of the literature applying pure bending, it can explain the differences of absolute values of results.

Chapter 5

Conclusions

This *in vitro* study was performed in order to understand if biological lesions injuries occurring in 50% of intervertebral discs, could alter the spine biomechanics. In addition, also *in vitro* biomechanical investigations of the disc surgery treatment, as discoplasty, sometimes require collateral lesions which could impact the surrounding tissues and alter the final outcome of the study.
To provide a response to this, eight thoraco-lumbar human spines were tested in flexion and extension in five different configurations with an worsening damage.

The sequential execution of axial and circumferential tears in the postero-lateral side on the IVD, did not alter significantly the spine biomechanics: neither bending stiffness, range of motion nor disc height were significantly changed by scalpel incision. This suggested that acute annular tears alone are not sufficient to induce off – axis motion and instability. In fact, in these cases, the nucleus pulposus deforms and redistributes the load to support the annulus.

Similarly, the annulus plug removal did not show significant effects with respect to the configuration with four cuts. It indicates that after the interruption of the fiber continuity, the presence or absence of the incised annulus material does not impact the IVD behavior.

The main effect caused by nucleotomy was the disc height reduction due to the lack of support caused by the nucleus loss.

The strain distribution on the disc surface showed also different pattern after nucleotomy for thoracic and lumbar levels in both the flexion and extension configuration. This confirmed the different disc behavior related to their location in the spine. In both cases, strains significantly changed in the last defect configuration, concentrating strains on smaller regions such as the mid-height line of the disc along the endplates. Combined with minimum compressive strains twice larger than in intact condition, nucleus removal

could make the annulus fibrosus vulnerable to fatigue damage and micro fractures. Contrary to previous studies, nucleus removal did not result in significantly different mechanical behavior.

This study emphasized the immediate consequences of disc injuries on the spine biomechanics and the long term damages the disc could undergo following such loss of integrity. This study only looked at the strain distribution over the disc surface but it would be also interesting to see if the superficial observation are still valid in the inside disc by using DVC to assess the 3D field of strains. Finally it is currently unknown how the AF incision site responds to applied load in terms of strains distribution and principal strain peaks. So DIC acquisition on the damaged side of the IVD could increase this knowledge.

Appendix A

Literature review on annulus tears in details

Reference	Specimen/ Spine Levels	AF Incision		NP removal
		Type	Location	
Cleason et al., 2019	Human, lumbar FSUs	Cruciate incision	Left postero-lateral region	30% of NP volume
Lee et al., 2018	Human, lumbar FSUs	Hole, ϕ = 3mm	Right postero-lateral region	As much as possible
Bostelmann et al., 2015	Human, lumbar FSUs	Rectangular window, 6x8 mm	Postero-lateral region	-
Ivicsics et al., 2014	Human, lumbar FSUs	Horizontal incision, 6-8 mm	Right postero-lateral region, in the mid-plane of the IVD	Partial NP removal and total removal
Showalter et al., 2014	Human, lumbar FSUs	Cruciform incision	Postero-lateral region	30% of NP volume
O'Connell et al., 2011	Human, lumbar FSUs	Cruciform incision	Postero-lateral region	20% of NP volume
Heuer et al., 2008	Human, lumbar FSUs	Oblique incision oreinted along a fiber direction	Right postero - lateral region	Total removal
Heuer et al., 2007	Human, lumbar FSUs	Oblique incision oreinted along a fiber direction	Right postero - lateral region	Total removal
Kuroki et al., 2004	Human, lumbar FSUs	Square window, 5x5 mm	Left posterior region	As much as possible
Frei et al., 2001	Human, lumbar FSUs	Vertical incision	Right postero-lateral region	As much as possible
Shea et al., 1994	Human, lumbar FSUs	Hole, incision	Right side	(Not specified)
Brinckmann et al., 1991	Human, lumbar FSUs	Incision	Dorso-lateral region	Different amount in different steps
Krismer et al., 1996	Human, lumbar FSUs	Cut following the fibers direction	-	-
Seroussi et al., 1989	Human, lumbar FSUs	Square window, 5x5 mm	Lateral region	A third of NP volume
Brinckmann et al, 1986	Human, lumbar FSUs	Radial incision + 2 additional horizontal cuts	Left dorso-lateral region	-
Goel et al., 1986	Human, lumbar FSUs	Horizontal incision	Posterior region	Small amount
Brinckmann et al, 1985	Human, lumbar FSUs	Incision	-	Part of the NP volume
Panjabi et al., 1984	Human, lumbar FSUs	Square window, 5x5 mm	Right postero-lateral region	As much as possible
Tencer et al, 1982	Human, lumbar FSUs	staggered horizontal cuts	Around the disc circumference, near both endplates	(No nucleus removal)

Reference	Test		Outcomes measurements setup
	Outcomes	Loading nature	
Cleason et al., 2019	Internal disc deformation field	Compression, stress - relaxation test	MRI
Lee et al., 2018	Axial stiffness, ROM	Axial compression and pure bending	3D motion analysis system
Bostelmann et al., 2015	Intradiscal pressure, ROM	Axial compression and bending	Pressure transducer, motion tracker system
Ivicsics et al., 2014	Load- displacement plot	Axial compression, flexion and extension	Displacement sensors
Showalter et al., 2014	Compression modulus, strains and disc height	Compressice cycling loading	MRI
O'Connell et al., 2011	Disc internal strains	Axial compression in flexion, neutral and extension position	MRI
Heuer et al., 2008	Disc surface strain, ROM	Pure bending moments in flexion, extension, lateral bending and axial rotation	Pins and laser scanner
Heuer et al., 2007	ROM	Pure bending moments in flexion, extension, lateral bending and axial rotation	Rotational potentiometers
Kuroki et al., 2004	ROM	Pure bending and Fatique test	Plexiglas markers with leds
Frei et al., 2001	Strain, disc pressure	Series of compression combined with F/E/LB and shear loads	Triaxial strain gauge
Shea et al., 1994	Intradiscal pressure, stiffness and disc geometry	Axial compression	LVDT
Brinckmann et al., 1991	Disc height, radial disc bulge and intradiscal pressure	Pure axial compression	Optoelectical transducers
Krismer et al., 1996	Load - displacement data	Pure axial rotational moments	-
Seroussi et al., 1989	Intra-disc displacement	Compression, flexion and extension tests	Stainless steel beads
Brinckmann et al, 1986	Disc Bulge	Pure axial compression	Transducers
Goel et al., 1986	Motionof the geometric center of the superior vertebra	Flexion, extension, lateral bending and axial torsion	Dial gauges
Brinckmann et al, 1985	Disc Bulge	Pure axial compression	Potentiometer transducers
Panjabi et al., 1984	Load- displacement plot	Flexibility and creep test	LVDT
Tencer et al, 1982	Load - displacement data	Flexion/extension and lateral bending	Electromechanical transducer

Appendix B

Average, minimum and maximum values of tensile and compressive strains over the disc surface in flexion and extension

FLEXION

	True principal strain 1 [με]			True principal strain 2 [με]		
	mean	min:	max:	mean	min:	max:
Sp. #1						
a)	4200	-503	19416	900	-5987	3566
b)	3800	-2641	23183	1000	-17600	7728
c)	3600	80	23741	1800	-9540	9743
d)	3000	-456	25664	2300	-12976	11414
e)	5400	-6694	46675	-10000	-52154	7511
Sp. #3						
a)	4300	-5421	28690	-5600	-50881	4931
b)	5200	-1546	35119	-10000	-67513	14807
c)	9100	-2948	43793	-20000	-75932	6944
d)	9000	-5558	42419	-20000	-86288	3774
e)	3500	-18570	51057	-30000	-108131	6360
Sp. #6						
a)	10000	734	41079	-8400	-34498	7125
b)	10000	1576	43646	-10000	-44431	8774
c)	10000	1229	41911	-10000	-44700	9475
d)	10000	-4807	46143	-20000	-53610	4601
e)	8200	-5075	26578	-30000	-101970	2473
Sp. #8						
a)	7100	-5484	30373	1900	-17807	8055
b)	7600	-911	38355	2500	-25801	10634
c)	8200	-2875	40402	2900	54381	11779
d)	7000	-10075	5147	1600	-84933	11375
e)	10000	-33022	1043	-7800	-123647	11576

	True principal strain 1 [με]			True principal strain 2 [με]		
	mean	min:	max:	mean	min:	max:
Sp. #2						
a)	2900	-6786	64744	-1800	-27810	12149
b)	3100	-7105	35591	-1300	-38157	6681
c)	3300	-8239	42604	-800	-30121	7223
d)	3300	-7096	26506	-1800	-31363	7171
e)	3000	-15563	36865	-8600	-69726	4831
Sp. #5						
a)	20000	-7572	75343	-10000	-80289	9534
b)	20000	-12873	70744	-20000	-117842	6078
c)	20000	-7337	89506	-10000	-107576	7324
d)	20000	-15505	48994	-20000	-147188	8776
e)	10000	-14197	84142	-40000	-207346	6492
Sp. #7						
a)	20000	2807	50460	-30000	-111028	5569
b)	10000	-14114	120199	-1000	-177577	13798
c)	10000	-19863	182885	-10000	-172415	7913
d)	10000	-3425	136803	-1000	-115122	4286
e)	7800	-5567	47722	-40000	-227528	2057
Sp. #4						
a)	20000	-12505	117858	-40000	-261868	17484
b)	20000	-24658	152714	-40000	-341929	5380
c)	10000	-4745	229468	-40000	-526149	17617
d)	20000	-45127	183748	-40000	-369746	12419
e)	20000	-66679	238396	-30000	-287926	5010

Average. minimum and maximum values of maximum and minimum strains over the disc surface in flexion.
Color code gathers the specimens by spine levels: purple: T9 – T10, blue: T10 - T11, yellow: T11 - T12, green: T12 - L1, red: L4 - L5.

EXTENSION

	True principal strain 1 [με]			True principal strain 2 [με]		
	mean	min:	max:	mean	min:	max:
Sp. #1						
a)	2900	-32987	22894	-3500	-49644	6155
b)	4100	-4106	16697	-900	-16805	5059
c)	3400	-3668	32958	-1900	-28516	4615
d)	3300	-5038	43110	-3600	-106345	5397
e)	4300	-9565	49118	-7700	53639	8683
Sp. #3						
a)	5500	-3382	2146	-10000	-67803	5588
b)	5500	-7141	30617	-10000	-67965	5109
c)	4600	-15331	42606	-10000	-96879	9784
d)	4200	-4582	37905	-10000	-9634	9646
e)	1200	-4594	26874	-9700	-93549	6177
Sp. #6						
a)	2040	-4568	33084	-4510	-73978	993
b)	2600	-3257	32764	-3100	-80614	4065
c)	2100	-2145	38054	-2900	-106808	3265
d)	5120	-1695	32232	-2300	-24808	4077
e)	5900	-3745	27271	-700	-31951	4513
Sp. #8						
a)	6800	-3059	44924	-5000	-39992	11128
b)	8200	-3942	40201	-5700	-33577	5995
c)	9700	-6400	57875	-6900	-86334	4199
d)	10000	-5081	67643	-10000	-124396	1768
e)	10000	-5768	86695	-20000	-133228	2876

	True principal strain 1 [με]			True principal strain 2 [με]		
	mean	min:	max:	mean	min:	max:
Sp. #2						
a)	3300	-9464	35592	-8700	-143022	5196
b)	2500	-9038	38089	-5800	-137118	4033
c)	3100	-12486	30322	-4100	-71499	9221
d)	2500	-12145	33805	-5700	-91775	8566
e)	5400	-27351	86440	-20000	-235012	-5826
Sp. #5						
a)	8800	-4789	168585	-1900	-54775	15934
b)	10000	-8414	86895	-900	-35228	13496
c)	20000	-1745	126811	700	-700	-28084
d)	20000	-8530	134820	1700	-101890	21992
e)	4900	-12806	46950	-5160	-98055	5124
Sp. #7						
a)	4800	-6137	71162	2000	-50526	12131
b)	8500	-3436	74852	3100	-96390	11352
c)	6800	-505	122905	2200	-85985	155776
d)	7000	-2633	92944	-4000	-99858	10461
e)	3600	-2864	32681	-2100	-60824	9607
Sp. #4						
a)	20000	-1658	152210	-9900	-174719	19583
b)	20000	-15565	273525	-9500	-155148	31238
c)	30000	-64391	162195	-20000	-217697	29568
d)	30000	-60760	119849	-10000	-222396	29941
e)	20000	-72334	141138	-10000	-255796	16833

Average. minimum and maximum values of maximum and minimum strains over the disc surface in extension.
Color code gathers the specimens by spine levels: purple: T9 – T10, blue: T10 - T11, yellow: T11 - T12, green: T12 - L1, red: L4 - L5.

References

- Adams, A., Roche, O., Mazumder, A., Davagnanam, I. & Mankad, K. Imaging of degenerative lumbar intervertebral discs; linking anatomy, pathology and imaging. *Postgrad Med J* 90, 511–519 (2014).

- Bostelmann, R., Steiger, H.-J. & Cornelius, J. F. Effect of Annular Defects on Intradiscal Pressures in the Lumbar Spine: An in Vitro Biomechanical Study of Diskectomy and Annular Repair. *J Neurol Surg A Cent Eur Neurosurg* 78, 46–52 (2017).

- Brinckmann, P. & Grootenboer, H. Change of disc height, radial disc bulge, and intradiscal pressure from discectomy. An in vitro investigation on human lumbar discs. *Spine* 16, 641–646 (1991).

- Brinckmann, P. & Horst, M. The influence of vertebral body fracture, intradiscal injection, and partial discectomy on the radial bulge and height of human lumbar discs. *Spine* 10, 138–145 (1985).

- Brinckmann, P. Injury of the annulus fibrosus and disc protrusions. An in vitro investigation on human lumbar discs. *Spine* 11, 149–153 (1986).

- Chung, S. M., Teoh, S. H., Tsai, K. T. & Sin, K. K. Multi-axial spine biomechanical testing system with speckle displacement instrumentation. *J Biomech Eng* 124, 471–477 (2002).

- Claeson, A. A. *et al.* Human Disc Nucleotomy Alters Annulus Fibrosus Mechanics at Both Reference and Compressed Loads. *J Biomech Eng* (2019) doi:10.1115/1.4043874.

- Cloyd, J. M. *et al.* Material properties in unconfined compression of human nucleus pulposus, injectable hyaluronic acid-based hydrogels and tissue engineering scaffolds. *Eur Spine J* 16, 1892–1898 (2007).

- Frei, H., Oxland, T. R., Rathonyi, G. C. & Nolte, L. P. The effect of nucleotomy on lumbar spine mechanics in compression and shear loading. *Spine* 26, 2080–2089 (2001).

- Galbusera, F. *et al.* Ageing and degenerative changes of the intervertebral disc and their impact on spinal flexibility. *Eur Spine J* 23 Suppl 3, S324-332 (2014).

- Goel, V. K., Nishiyama, K., Weinstein, J. N. & Liu, Y. K. Mechanical properties of lumbar spinal motion segments as affected by partial disc removal. *Spine* 11, 1008–1012 (1986).

- Gray H. Gray's anatomy, 41ª ed., Elsevier, 2016.

- Green, T. P., Adams, M. A. & Dolan, P. Tensile properties of the annulus fibrosus II. Ultimate tensile strength and fatigue life. *Eur Spine J* 2, 209–214 (1993).

- Gustafson, H., Siegmund, G. & Cripton, P. Comparison of Strain Rosettes and Digital Image Correlation for Measuring Vertebral Body Strain. *J Biomech Eng* 138, 54501 (2016).

- Heuer, F., Schmidt, H., Klezl, Z., Claes, L. & Wilke, H.-J. Stepwise reduction of functional spinal structures increase range of motion and change lordosis angle. *J Biomech* 40, 271–280 (2007).

- Heuer, F., Schmidt, H. & Wilke, H.-J. Stepwise reduction of functional spinal structures increase disc bulge and surface strains. *J Biomech* 41, 1953–1960 (2008).

- Ignasiak, D., Dendorfer, S. & Ferguson, S. J. Thoracolumbar spine model with articulated ribcage for the prediction of dynamic spinal loading. *J Biomech* 49, 959–966 (2016).

- Ivicsics, M. F., Bishop, N. E., Püschel, K., Morlock, M. M. & Huber, G. Increase in facet joint loading after nucleotomy in the human lumbar spine. *J Biomech* 47, 1712–1717 (2014).

- Karakolis, T. & Callaghan, J. P. Localized strain measurements of the intervertebral disc annulus during biaxial tensile testing. *Comput Methods Biomech Biomed Engin* 18, 1737–1743 (2015).

- Kirkaldy-Willis, W. H. & Farfan, H. F. Instability of the lumbar spine. *Clin. Orthop. Relat. Res.* 110–123 (1982).

- Kiss, L. *et al.* Indirect foraminal decompression and improvement in the lumbar alignment after percutaneous cement discoplasty. *Eur Spine J* 28, 1441–1447 (2019).

- Krismer, M., Haid, C., Ogon, M., Behensky, H. & Wimmer, C. [Biomechanics of lumbar instability]. *Orthopade* 26, 516–520 (1997).

- Krismer, M., Haid, C. & Rabl, W. The contribution of anulus fibers to torque resistance. *Spine* 21, 2551–2557 (1996).

- Kuroki, H. *et al.* Contributions of flexion-extension cyclic loads to the lumbar spinal segment stability following different discectomy procedures. *Spine* 29, E39-46 (2004).

- Lee, T., Lim, T.-H., Lee, S.-H., Kim, J.-H. & Hong, J. Biomechanical function of a balloon nucleus pulposus replacement system: A human cadaveric spine study. *J. Orthop. Res.* 36, 167–173 (2018).

- Liao, D., Wang, P., Zhao, J. & Gregersen, H. Validation of Shape Context Based Image Registration Method Using Digital Image Correlation Measurement on a Rat Stomach. *Journal of Computational Medicine* https://www.hindawi.com/journals/jcm/2014/504656/ (2014).

- Michalek, A. J. & Iatridis, J. C. Height and torsional stiffness are most sensitive to annular injury in large animal intervertebral discs. *Spine J* 12, 425–432 (2012).

- Newell, N. *et al.* Biomechanics of the human intervertebral disc: A review of testing techniques and results. *J Mech Behav Biomed Mater* 69, 420–434 (2017).

- O'Connell, G. D., Malhotra, N. R., Vresilovic, E. J. & Elliott, D. M. The effect of nucleotomy and the dependence of degeneration of human intervertebral disc strain in axial compression. *Spine* 36, 1765–1771 (2011).

- Osti, O. L., Vernon-Roberts, B. & Fraser, R. D. 1990 Volvo Award in experimental studies. Anulus tears and intervertebral disc degeneration. An experimental study using an animal model. *Spine* 15, 762–767 (1990).

- Palanca, M., Brugo, T. M. & Cristofolini, L. Use of digital image correlation to investigate the biomechanics of the vertebra. *J. Mech. Med. Biol.* 15, 1540004 (2015).

- Palanca, M., Marco, M., Ruspi, M. L. & Cristofolini, L. Full-field strain distribution in multi-vertebra spine segments: An in vitro application of digital image correlation. *Med Eng Phys* 52, 76–83 (2018).

- Palanca, M., Tozzi, G. & Cristofolini, L. The use of digital image correlation in the biomechanical area: a review. *International Biomechanics* 3, 1–21 (2016).

- Panjabi, M. M., Krag, M., Summers, D. & Videman, T. Biomechanical time-tolerance of fresh cadaveric human spine specimens. *J. Orthop. Res.* 3, 292–300 (1985).

- Panjabi, M. M., Krag, M. H. & Chung, T. Q. Effects of disc injury on mechanical behavior of the human spine. *Spine* 9, 707–713 (1984).

- Raj, P. P. Intervertebral disc: anatomy-physiology-pathophysiology-treatment. *Pain Pract* 8, 18–44 (2008).

- Ross, S.M. Peirce's criterion for the elimination of suspect experimental data. *Journal of Engineering Technology* 2003.

- Ruspi, M. L., Palanca, M., Faldini, C. & Cristofolini, L. Full-field in vitro investigation of hard and soft tissue strain in the spine by means of Digital Image Correlation. *Muscles Ligaments Tendons J* 7, 538–545 (2017).

- Seroussi, R. E., Krag, M. H., Muller, D. L. & Pope, M. H. Internal deformations of intact and denucleated human lumbar discs subjected to compression, flexion, and extension loads. *J. Orthop. Res.* 7, 122–131 (1989).

- Shea, M., Takeuchi, T. Y., Wittenberg, R. H., White, A. A. & Hayes, W. C. A comparison of the effects of automated percutaneous diskectomy and conventional diskectomy on intradiscal pressure, disk geometry, and stiffness. *J Spinal Disord* 7, 317–325 (1994).

- Showalter, B. L., Malhotra, N. R., Vresilovic, E. J. & Elliott, D. M. Nucleotomy reduces the effects of cyclic compressive loading with unloaded recovery on human intervertebral discs. *J Biomech* 47, 2633–2640 (2014).

- Siebert, T., Becker, T., Spiltthof, K., Neumann, I. & Krupka, R. Error Estimations in Digital Image Correlation Technique. *Applied Mechanics and Materials* https://www.scientific.net/AMM.7-8.265 (2007).

- Sola, C. *et al.* Percutaneous cement discoplasty for the treatment of advanced degenerative disk disease in elderly patients. *Eur Spine J* (2018) doi:10.1007/s00586-018-5547-7.
- Spera, D., Genovese, K. & Voloshin, A. Application of Stereo-Digital Image Correlation to Full-Field 3-D Deformation Measurement of Intervertebral Disc. *Strain* 47, e572–e587 (2011).
- Tanaka, N. *et al.* The relationship between disc degeneration and flexibility of the lumbar spine. *Spine J* 1, 47–56 (2001).

- Techens C., Palanca M., Eltes P.E., Lazary A., Cristofolini L. What is the impact of discoplasty treatment on degenerated intervertebral discs? Submitted.

- Tencer, A. F., Ahmed, A. M. & Burke, D. L. Some static mechanical properties of the lumbar intervertebral joint, intact and injured. *J Biomech Eng* 104, 193–201 (1982).

- Thompson, R. E. *et al.* Disc lesions and the mechanics of the intervertebral joint complex. *Spine* 25, 3026–3035 (2000).

- Thompson, R. E., Pearcy, M. J. & Barker, T. M. The mechanical effects of intervertebral disc lesions. *Clin Biomech (Bristol, Avon)* 19, 448–455 (2004).

- Varga, P. P., Jakab, G., Bors, I. B., Lazary, A. & Szövérfi, Z. Experiences with PMMA cement as a stand-alone intervertebral spacer: Percutaneous cement discoplasty in the case of vacuum phenomenon within lumbar intervertebral discs. *Orthopade* 44 Suppl 1, S1-7 (2015).

- Wilke, H. J., Wenger, K. & Claes, L. Testing criteria for spinal implants: recommendations for the standardization of in vitro stability testing of spinal implants. *Eur Spine J* 7, 148–154 (1998).

Ringraziamenti

Anche se ancora non mi sembra vero, eccomi arrivata alla fine di questo lungo e complicato percorso.

Per prima cosa vorrei ringraziare il professor Cristofolini per avermi permesso di svolgere la tesi all'interno del suo laboratorio di Biomeccanica, facendomi entrare nell'affascinante mondo della ricerca, e per avermi affidato un progetto che rispecchiava esattamente quello che mi sarebbe piaciuto fare. È stata per me una bella sfida, spero di esserne stata all'altezza.

Grazie Chloé, per avermi seguito passo a passo, dall'inizio alla fine, guidandomi ogni giorno tra la preparazione dei provini, i test meccanici, l'analisi dei risultati e i continui imprevisti sempre dietro l'angolo. Grazie perché in ogni momento di difficoltà e insicurezza mi hai dato coraggio spronandomi a credere sempre in me stessa. Grazie soprattutto per la pazienza e per aver dovuto ascoltare il mio inglese!

Grazie Toti, per tutti gli infiniti piaceri che ti ho chiesto, per le chiacchiere e gli sfoghi!..Non so come farai ora senza che qualcuno ti chieda continuamente la connessione a TeamViewer ;)

Grazie a tutti i ragazzi, i dottorandi e i tecnici del laboratorio, che tra un passaggio in stazione, un pranzo, un saluto in corridoio o davanti alla macchina di prova, mi hanno sempre fatto sentire come parte integrante del laboratorio, e non solo come una tesista.

Grazie alla mia famiglia, perché starmi accanto negli ultimi anni non deve essere stato facile, e per aver rispettato la mia poca voglia di ricevere domande e dare risposte.

Grazie Matteo, per essermi stato sempre accanto, per avermi supportato incondizionatamente e per avere capito e rispettato i miei *'stammi vicino, ma lontano, che devo studiare'*. Grazie per tutti i bellissimi momenti passati insieme, per aver asciugato le mie lacrime nei momenti di crisi e per essere sempre corso da me ogni volta che avevo bisogno di un abbraccio. Grazie per aver sopportato i miei sfoghi e per avere sempre

trovato le parole giuste per farmi sorridere… sei stato fondamentale, soprattutto in questo ultimo periodo!
… e grazie per i tuoi bellissimi disegni dei dischi intervertebrali :)

Grazie Vale e Lo, per aver creduto in me più di quanto abbia fatto io stessa. Grazie per il sostegno e per esserci sempre state! Ho già in mente qualche meta per i nostri prossimi weekend ;)

Grazie a tutti i miei compagni di corso per aver condiviso con me lezioni, laboratori, tesine e relazioni. I momenti passati insieme sono stati i più belli.

Grazie a tutti coloro che ci sono sempre stati, e a chi, anche solo con un messaggio o con poche parole mi ha sostenuto e dato coraggio!

Grazie a tutti!
Sara

P.s.: ora, nonna Anita, spero finalmente di poter rispondere alla tua domanda: ‘ma io non ho mica capito, quindi che lavoro farai dopo la laurea?’